ELSEVIER

Chemical Geology 199 (2003) 293–315

CHEMICAL GEOLOGY
INCLUDING
ISOTOPE GEOSCIENCE

www.elsevier.com/locate/chemgeo

A Permian underplating event in late- to post-orogenic tectonic setting. Evidence from the mafic–ultramafic layered xenoliths from Beaunit (French Massif Central)

Olivier Féménias[a,b,*], Nicolas Coussaert[b,c], Bernard Bingen[d], Martin Whitehouse[e], Jean-Claude C. Mercier[b], Daniel Demaiffe[a]

[a] *Laboratoire de Géochimie Isotopique et Géodynamique Chimique, DSTE, Université Libre de Bruxelles (CP 160/02), 50 Avenue Roosevelt, 1050 Brussels, Belgium*
[b] *Université de La Rochelle, av. Crépeau, 17402 La Rochelle cedex 1, France*
[c] *Unité de Minéralogie et Géochimie, Musée Royal de l'Afrique Centrale, B-3080 Tervuren, Belgium*
[d] *Geological Survey of Norway, 7491 Trondheim, Norway*
[e] *Laboratory for Isotope Geology, Swedish Museum of Natural History, Box 50007, 104 05 Stockholm, Sweden*

Received 24 September 2002; accepted 31 March 2003

Abstract

The Puy Beaunit volcano vent, French Massif Central, displays a population of plutonic mafic to ultramafic xenoliths, commonly showing asymmetric, millimetre to centimetre thick, layering. Layers are pyroxenitic to gabbroic, and less commonly peridotitic (lherzolite, dunite, websterite) and anorthositic. These xenoliths are interpreted as samples of a layered intrusion, located at the crust–mantle boundary. Primary cumulate phases are olivine and orthopyroxene, followed by clinopyroxene and plagioclase; rare intercumulus accessory phases (apatite, rutile and zircon) are observed in the most differentiated layers. Homogeneous xenoliths, interpreted as single cumulate layers, have a calc-alkaline geochemistry with LREE and large ion lithophile elements (LILE) enrichments relative to Nb, Ta and Ti. The negative Eu anomaly of pyroxenite can be related to earlier plagioclase fractionation, as observed in the gabbroic layers. Trace element laser ablation inductively coupled plasma emission mass spectrometry (LA-ICP-MS) and secondary ion mass spectrometry (SIMS) analyses of plagioclase, orthopyroxene and zircon from layered rocks suggest equilibrium and cogenetic relations between the silicate phases. U–Pb SIMS dating of a 1.5 mm zircon crystal gives a magmatic or sub-solidus equilibration age of 257 ± 6 Ma.

The Beaunit layered intrusion belongs to the large Permian within-plate magmatic episode commonly of calc-alkaline geochemical signature observed over Europe and North Africa. It probably corresponds to a mafic underplating event spatially controlled by post-Variscan trans-tensional to trans-pressional basin tectonics in an intracontinental setting. The subduction-related geochemical signature of the magmatic suite is interpreted as resulting from the passive remobilisation of a mantle source, which was previously metasomatised during the Variscan subduction.
© 2003 Elsevier Science B.V. All rights reserved.

Keywords: Massif Central; Permian; Zircon; Ultramafic–mafic xenolith; Layered intrusion; Calc-alkaline magmatism

* Corresponding author. Laboratoire de Géochimie Isotopique et Géodynamique Chimique, DSTE, Université Libre de Bruxelles (CP 160/02), 50 Avenue Roosevelt, 1050 Brussels, Belgium. Tel.: +32-2-650-22-54; fax: +32-2-650-22-26.
E-mail address: ofemenia@ulb.ac.be (O. Féménias).

0009-2541/03/$ - see front matter © 2003 Elsevier Science B.V. All rights reserved.
doi:10.1016/S0009-2541(03)00124-4

1. Introduction

Cenozoic alkaline volcanoes of the Massif Central (France) carry a large variety of xenoliths derived from the crust and the upper mantle. The geochemistry, petrology and texture of layered crustal granulites and mantle-derived ultramafic peridotites have been intensively studied (Leyreloup, 1973; Porcelli et al., 1986 and references in Féménias et al., 2001). These studies have shed some light on the composition and origin of the deep continental lithosphere. Xenoliths derived from deep layered intrusions have been identified but rarely described in a given occurrence. This paper describes a xenolith population of magmatic origin in the Puy Beaunit vent. Beaunit is a quaternary maar, dated at 43,900 ± 5100 years (Rosseel, 1996 in Faure et al., 2001), occurring at the northernmost end of Chaîne des Puys (Fig. 1B). The scoria cone of Beaunit (puy Gonnard) contains abundant and varied mantle and crustal xenoliths; it represents one of the richest occurrences with respect to xenolith diversity (Brousse and Rudel, 1964; Mercier, 1972; Leyreloup, 1973). Recently, Féménias et al. (2001) provided preliminary geochemical and textural data on the Puy Beaunit xenoliths. They described a large range of mafic to ultramafic xenoliths of plutonic origin, some of them with well-defined layering. Primary equilibrium conditions obtained from orthopyroxene–clinopyroxene pairs in ultramafic xenoliths (Féménias et al., 2001) and secondary pyrometamorphic history deduced from a detailed nanopetrographic investigation on a single mafic xenolith (Faure et al., 2001) permit to infer the existence of a layered intrusion at a depth of some 30 km, close to the crust–mantle boundary in that area (Zeyen et al., 1997 and references in Faure et al., 2001). Goër de Herve et al. (1991) interpreted the mafic magmatic nodules as fragments of the magma chamber beneath the Quaternary volcano. However, Sr–Nd iso-

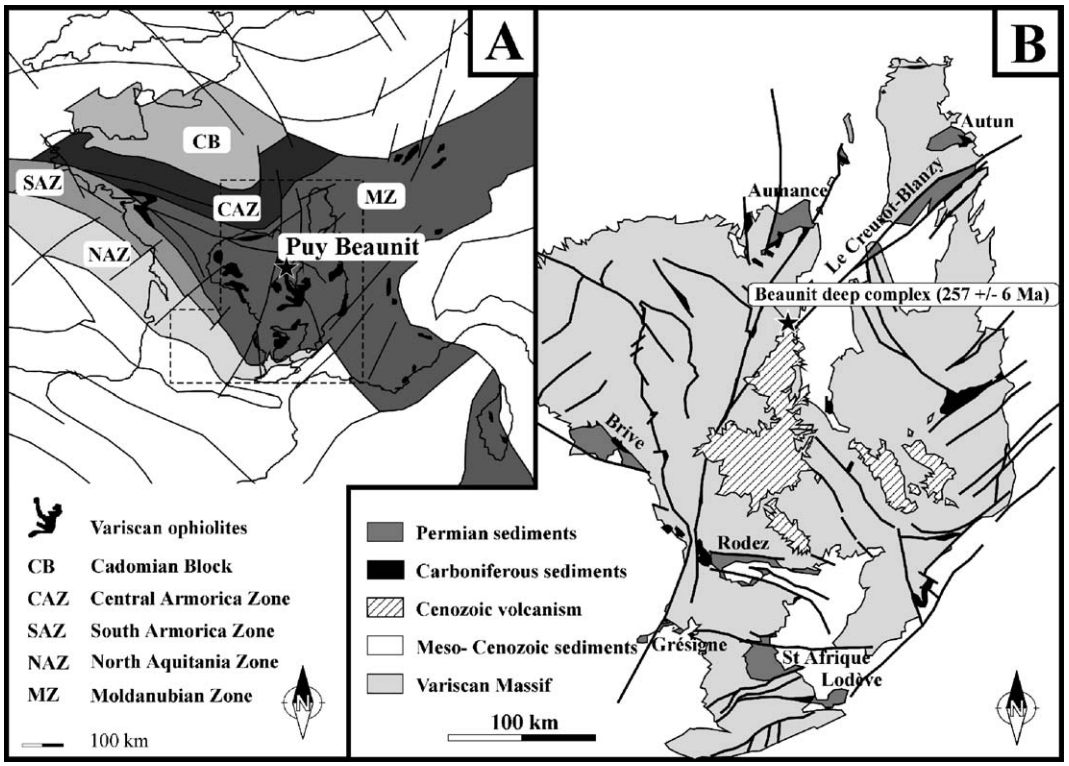


Fig. 1. Beaunit geotectonic setting. (A) Basement tectonic sketch map of western Europe (modified after Chantraine et al., 1996). (B) Structural map of the French Massif Central during the Permian period showing the location and extension of the Permian and Carboniferous basins and of the Cenozoic volcanism.

topic studies on the pyroxenitic nodules (Downes and Dupuy, 1987) do not show any relations with the recent alkaline basalt and point either to a mantle or lower crustal signature (Downes et al., 1990). The mode of emplacement, the differentiation processes and the geotectonic implications of the deep magmatic complex from Beaunit have remained largely unknown.

In this paper, we present new petrological and geochemical data on a selected population of ultramafic and mafic plutonic nodules, some of them displaying a well-defined layered texture. Whole rock analyses and in situ trace element analyses of minerals by laser ablation inductively coupled plasma emission mass spectrometry (LA-ICP-MS) and secondary ion mass spectrometry (SIMS) are combined with previously obtained secondary electron microprobe data to better constrain the cumulative origin of these rocks. In the course of this study, a large zircon crystal was discovered in a layered xenolith of gabbro–orthopyroxenite composition (sample PNB00-01). This crystal has been dated by in situ U–Pb isotopic analyses by SIMS and yields a Permian age of 257 ± 6 Ma. The geochemical affinity and the intrusion age of the Beaunit deep layered intrusion will be discussed in the context of the late- to post-collisional evolution of the internal zone of the Variscan orogeny.

2. Analytical methods

The ultramafic–mafic plutonic xenoliths selected for this study are described in the following section. The modal proportions of orthopyroxene, clinopyroxene, olivine, spinel and plagioclase were determined by image analysis on thick polished sections (150 μm). Ultramafic xenoliths have been classified and named using the IUGS international classification (Streckeisen, 1974; Le Maitre, 1989). Major element compositions of olivine, clinopyroxene, orthopyroxene, plagioclase and spinel have been determined by electron microprobe on Camebax and SX50 instruments at Paris VI University (France) using a combination of natural and synthetic mineral standards. The operating conditions involve an accelerating voltage of 15 kV, a beam current of 10 nA and a count time of 10 s per element for major mineral phases.

Samples selected for whole-rock major and trace elements have been crushed and ground in a stainless steel mortar. Whole-rock X-ray fluorescence (XRF) spectrometric analyses of major elements and Cr were made on fused glass discs at Liège University (Collectif de Géochimie instrumentale). Samples were preignited at 1000 °C during 3 h, so major elements are reported on a volatile-free basis and total iron is reported as Fe_2O_3 (tot). Upon ignition, the peridotites and some pyroxenites have a small weight gain (0.08% to 0.86%) due to the iron oxidation. The XRF measurements were calibrated using 22 international standards and tested on three ultramafic standards (JP1, NIM-D, NIM-P) that are comparable to the studied rocks. The typical precision and accuracy (illustrated by the Relative Standard Deviation, RSD) for the major elements XRF analyses range from 0.1 to 2%, except for Na_2O and TiO_2 that have low concentrations (< 0.05 wt.%). The data are given in Table 1 and compared to the recommended values (Govindaraju, 1994). Some trace elements (Ni, Cu, Zn, V and Sr) were measured by X-ray fluorescence spectrometry on pressed powder pellets. Other trace elements (Rb, Cs, Ba, Zr, Hf, Nb, Ta, U, Th, Pb, Y, and the rare earth elements, REEs) were analysed using a VG Elemental Plasma Quad PQ2 ICP-MS at the "Collectif de Géochimie instrumentale". Rock samples were dissolved by alkali fusion. The procedure used there (Vander Auwera et al., 1998) is the same as that described by Totland et al. (1992). The ICP-MS measurements were calibrated using 5 international standards including the peridotite JP1 and tested on the two ultramafic NIM standards (NIM-D, NIM-P). Each standard has been analysed twice during measurement procedure. The limits of quantitative determination (LOQ: background + 10σ on 11 determinations of the signal produced by a "blank reagent" containing $LiBO_2$, HNO_3 and H_2O) are similar to those proposed in the literature (Jarvis, 1990). Accuracy of the method for ultramafic standards is usually good (< 15%) except for MREE (< 25%) and Pb (38%) that are closed to LOG in ultramafic standards. Table 1 gives the NIM results and the data of Pin and Joannon (1997) for comparison. The whole rock geochemical data are reported in Table 2.

The trace elements were analysed in orthopyroxene and plagioclase from two layered xenoliths using in situ LA-ICP-MS. The data were collected with a UV Fisons laser ablation microprobe coupled to a VG

Table 1
Major (wt.%), and traces (ppm) analyses for the two NIM ultramafic standards

	NIM-D measured	NIM-D reference	NIM-P measured	NIM-P reference
Major elements (wt.%)				
SiO_2	38.87	**38.96**	50.94	**51.10**
TiO_2	0.03	**0.02**	0.21	**0.20**
Al_2O_3	0.23	**0.30**	4.14	**4.18**
Fe_2O_3t	16.79	**16.96**	12.56	**12.76**
MnO	0.21	**0.22**	0.23	**0.22**
MgO	43.10	**43.51**	25.59	**25.33**
CaO	0.28	**0.28**	2.70	**2.66**
Na_2O	0.01	**0.04**	0.38	**0.37**
K_2O	0.01	**0.01**	0.09	**0.09**
P_2O_5	0.01	**0.01**	0.02	**0.02**
Trace element (ppm)				
Ni	2051	**2050**	555	**560**
Cr	2947	**2900**	24,101	**24,000**
La	0.210	**0.101**	1.94	**1.93**
Ce	0.201	**0.160**	4.23	**3.94**
Pr	0.020	**0.016**	0.536	**0.471**
Nd	0.093	**0.126**	1.90	**1.92**
Sm	0.024	**0.037**	0.460	**0.424**
Eu	0.005	**0.0027**	0.161	**0.129**
Gd	0.020	**0.0135**	0.501	**0.488**
Tb	0.003	**0.0024**	0.077	**0.0775**
Dy	0.029	**0.0186**	0.478	**0.514**
Ho	0.006	**0.0051**	0.113	**0.113**
Er	0.027	**0.0206**	0.372	**0.343**
Tm	0.005	**0.0047**	0.052	**0.059**
Yb	0.040	**0.0416**	0.388	**0.402**
Lu	0.008	**0.0089**	0.061	**0.0692**

Ni, Cr were measured by XRF and the rare earth elements by ICP-MS. Values for the major elements compiled by Govindaraju (1994) and the REE abundances determined by Pin and Joannon (1997) for these standards are given for comparison (in bold faces).

Elemental Plasma Quad (PQ2 Turbo Plus) ICP-MS (M.R.A.C. Tervuren). Data are given in Table 3. The laser ablation microprobe used in this study is based on a Continuum Minilite Q-switched Nd:YAG laser operating in the far-UV (266 nm) wavelength. The power of output beam is maximum (2 mJ/pulse) for a 10 Hz repetition rate of pulse, that is attenuated in agreement with the appropriate energy to the crater size required. These craters are in the range 40 to 60 μm. The focusing on the sample is done manually through a high magnification lens (1500 ×). Each sample and standard was ablated during 27 s corresponding to 12 s of pre-ablation to clean the surface and stabilise the ablation, followed by 15 s of data acquisition. The raw data on each isotope peak were subtracted from the gas blanks and normalised to the ^{43}Ca signal and then compared to calibration lines. The calibration lines are based on the NIST 612 and NIST 610 synthetic glass standards and two laboratory mineral standards: a pyrope megacryst from the Shavaryn–Tsaram basalts (Mongolia) and a Cr-diopside from the Inagly dunite massif (Siberia) to constrain the matrix effects. Typical theoretical detection limits for semi-quantitative analyses (>background + 3σ) are in the range 10–20 ppb for Y, Zr, Nb, Ba, Ta, La, Ce, Pr, Eu, Er, Yb and Lu, 30–50 ppb for Sr, Nd, Sm and Gd, 100 ppb for Pb, 400 ppb for V, 700 ppb for Co, 1–7 ppm for transition elements (Sc, Ti, Cr and Ni). The typical precision and accuracy for a laser microprobe analysis (calculated on 10 analyses of NIST 612 and five to seven analyses for natural crystals) range from 2% to 15% for NIST 612 and 6% to 18% for plagioclase and orthopyroxene of this study. The low Ta, La and Eu contents of orthopyroxenes are generally near or slightly below the semi-quantitative detection limits, their contents are given as indicative values and will be not discussed.

In situ U–Th–Pb age determinations were performed by secondary ion mass spectrometry (SIMS) on the zircon crystal found in sample PBN 00-01. We used a Cameca IMS 1270 instrument (Nordsim Laboratory, Swedish Museum of Natural History, Stockholm) for analyses, with a spot size of ca. 30 μm (Whitehouse et al., 1997, 1999). The analytical methods, data reduction, error propagation and assessment of the results are given in Whitehouse et al. (1997, 1999). The analyses were conducted with a ca. 4 nA O_2^- beam. A long analytical routine (ca. 30 min) provides optimal counting statistics for Palaeozoic zircons. The U/Pb ratio was calibrated using five analyses of the Geostandard 91,500 reference zircon (Wiedenbeck et al., 1995) on the same mount. The error on the U/Pb ratio includes propagation of the error related to the calibration curve. No common Pb (Pb_c) correction was applied. The data are reported in Table 4 and calculated according to the Isoplot program (Ludwig, 1999). Trace element analyses of REE, Y and Hf were carried out on the same zircon crystal in two of the pits left after Th–U–Pb analyses. Data were obtained with the same SIMS instrument operating under energy filtering conditions at low mass resolution. The concentrations were calibrated using the NIST 610 reference glass, the complete analytical

Table 2
Bulk rock analyses of representative spinel-bearing ultramafic xenoliths from Beaunit

Sample	PBN 86-19	PBN 98-39	PBN 98-01	PBN 98-09	PBN 86-24	PBN 98-05	PBN 98-13	PBN 98-27	PBN 98-54
Rock type	Opx-wb	Opx-wb	Cpx-wb	Ol-wb	Lz	Lz	Hz	Hz	Du
Modal proportions (opx, cpx, ol)									
Opx	82.9	73.1	18.8	23.9	45.7	23.7	19.7	14.6	3.0
Ol	1.1	5.2	0.0	35.2	42.6	48.0	79.0	83.8	96.8
Cpx	16.0	21.7	81.2	40.9	11.7	28.2	1.3	1.5	0.2
Major elements (wt.%)									
SiO_2	53.68	52.81	53.47	49.64	49.41	48.05	43.62	43.21	39.69
TiO_2	0.19	0.33	0.12	0.07	0.18	0.06	0.08	0.05	0.04
Al_2O_3	2.01	2.36	2.79	1.89	2.77	1.06	1.88	0.64	0.15
Fe_2O_3t	11.76	13.15	7.12	10.99	8.74	9.35	8.75	11.90	14.67
MnO	0.22	0.24	0.17	0.20	0.16	0.16	0.13	0.17	0.19
MgO	27.90	26.53	20.89	29.93	35.49	34.61	42.61	43.08	44.39
CaO	3.32	4.54	15.04	7.32	2.67	6.26	1.94	0.54	0.06
Na_2O	0.52	0.34	0.41	0.12	0.37	0.13	0.14	0.01	0.01
K_2O	0.05	0.11	0.03	0.01	0.14	0.01	0.08	0.01	0.01
P_2O_5	0.01	0.03	0.02	0.01	0.03	0.01	0.02	0.01	0.01
LOI	− 0.42	0.00	0.06	− 0.08	− 0.26	0.28	0.00	− 0.25	− 0.86
Sum	99.7	100.4	100.1	100.2	100.0	99.7	99.3	99.6	99.2
$Mg^{\#}$	0.73	0.69	0.77	0.75	0.82	0.80	0.84	0.80	0.77
Trace element (ppm)									
Ni	312	2031	202	2035	1701	1899	523	511	1853
Cr	2763	3281	2730	2698	2350	3259	2602	5455	2712
Cu	7	12	15	9	8	28	9	12	7
Zn	110	76	39	70	58	70	62	112	81
V	137	151	207	154	63	115	59	66	35
Rb	2.5	4.0	2.0	1.5	5.0	1.2	1.4	1.3	1.1
Cs	0.08	0.08	0.06	0.06	0.16	0.05	0.06	0.04	0.05
Sr	16.4	37.8	50.4	18.8	56.0	38.9	10.2	4.02	2.95
Ba	27	40	27	27	65	11	14	7	9
Zr	7.9	17.8	12.9	7.7	13.3	6.0	1.4	2.5	4.9
Hf	0.35	0.46	0.33	0.23	0.47	0.19	0.08	0.11	0.11
Nb	1.01	3.32	2.40	0.72	3.61	0.58	0.38	0.30	0.61
Ta	0.08	0.17	0.08	0.02	0.19	0.03	0.01	0.01	0.03
U	0.15	0.14	0.10	0.05	0.17	0.09	0.08	0.03	0.05
Th	0.36	0.50	0.30	0.99	0.58	0.28	0.29	0.14	0.12
Pb	4.73	1.57	1.10	1.11	1.29	1.21	1.22	0.82	0.77
Y	2.62	4.74	2.09	3.42	3.37	2.36	1.01	0.28	0.42
La	1.68	4.05	2.14	1.76	4.45	3.73	1.05	0.23	0.42
Ce	4.57	6.75	5.03	3.65	8.68	7.03	1.75	0.64	0.49
Pr	0.67	0.98	0.51	0.36	0.99	0.87	0.25	0.07	0.05
Nd	3.49	3.80	2.11	1.31	4.07	3.82	1.01	0.25	0.19
Sm	0.93	0.97	0.38	0.34	0.80	0.77	0.15	0.04	0.06
Eu	0.15	0.21	0.15	0.13	0.25	0.11	0.05	0.01	0.02
Gd	0.77	0.91	0.34	0.42	0.73	0.56	0.19	0.04	0.07
Tb	0.10	0.14	0.06	0.08	0.10	0.07	0.03	0.01	0.01
Dy	0.53	0.81	0.35	0.51	0.57	0.38	0.19	0.05	0.08
Er	0.27	0.51	0.22	0.32	0.30	0.21	0.13	0.04	0.06
Yb	0.26	0.50	0.20	0.32	0.29	0.20	0.12	0.06	0.08
Lu	0.04	0.07	0.04	0.05	0.04	0.03	0.02	0.01	0.01
$(Eu/Eu^*)_N$	0.54	0.68	1.30	1.08	1.01	0.51	0.88	1.01	0.95

Major elements by XRF; trace elements by XRF or ICP-MS, rare earth elements (REE) by ICP-MS. Rock type: Lz = lherzolite; Hz = harzburgite; Du = dunite; Opx-wb = orthopyroxene-rich websterite; Cpx-wb = clinopyroxene-rich websterite; Ol-wb = olivine-rich websterite.

Table 3
Representative LA-ICP-MS analyses of plagioclase and orthopyroxene and SIMS analyses of zircon from layered xenoliths from Beaunit (n = number of spots)

Sample	PBN 00-03										Sample PBN 00-01											
Mineral	plagio	opx	opx	plagio	opx	opx	opx	opx	plagio	opx	plagio	opx	opx	opx	opx	opx	opx	opx	opx	opx	zircon	zircon
Spot #	ac (n=5)	ad (n=4)	af (n=5)	ai (n=5)	al (n=5)	am (n=5)	an (n=5)	au (n=5)	av (n=4)	ay (n=4)	1 (n=5)	a (n=5)	b (n=5)	c (n=6)	d (n=5)	e (n=5)	f (n=5)	g (n=5)	h (n=5)	i (n=5)	a	c
Results (in ppm) by LA-ICP-MS (plagioclase and orthopyroxene) and SIMS (zircon)																						
Sc	9.7	4.3	12.4	6.6	13.6	6.3	7.9	5.9	3.6	8.1	–	–	–	–	–	–	–	–	–	–	–	–
Ti	193	283	525	272	342	463	810	536	188	493	–	–	–	–	–	–	–	–	–	–	–	–
V	13	84	142	13	104	59	73	58	6	100	–	–	–	–	–	–	–	–	–	–	–	–
Cr	79	280	441	54	417	533	695	511	38	744	–	–	–	–	–	–	–	–	–	–	–	–
Co	4	14	23	4	23	16	21	14	52	23	–	–	–	–	–	–	–	–	–	–	–	
Ni	31	16	44	22	53	31	67	31	663	57	–	–	–	–	–	–	–	–	–	–	–	–
Sr	1214	16.5	2.98	1485	1.53	0.99	0.83	0.68	1040	8.22	–	–	–	–	–	–	–	–	–	–	–	–
Ba	49	0.7	2.2	181	0.3	0.2	0.5	0.7	53.6	4.3	–	–	–	–	–	–	–	–	–	–	–	–
Pb	2.8	0.2	0.2	4.7	0.3	0.1	0.2	0.1	2.0	0.3	–	–	–	–	–	–	–	–	–	–	–	–
Zr	1.57	5.48	9.71	2.98	4.97	7.62	10.93	8.63	3.20	8.67	–	–	–	–	–	–	–	–	–	–	–	–
Hf	0.14	0.18	0.37	0.13	0.32	0.39	0.43	0.25	0.10	0.34	–	–	–	–	–	–	–	–	–	–	11,491	10,996
Nb	0.05	<	0.16	0.32	0.02	0.01	0.03	0.09	0.52	0.14	–	–	–	–	–	–	–	–	–	–	–	–
Ta	0.03	<	0.01	0.02	<	0.01	0.01	0.01	0.02	<	–	–	–	–	–	–	–	–	–	–	–	–
Y	3.21	4.40	7.89	4.89	6.60	4.36	5.72	5.44	3.54	5.23	–	–	–	–	–	–	–	–	–	–	207.8	208.0
La	5.68	0.03	0.04	6.77	0.01	0.02	0.02	0.03	5.84	0.03	16.53	0.14	0.08	0.03	0.02	0.03	0.03	0.04	0.17	0.08	0.16	0.14
Ce	10.50	0.09	0.13	12.39	0.07	0.08	0.11	0.14	8.83	0.12	32.60	0.10	0.44	0.14	0.09	0.23	0.10	0.18	0.32	0.20	3.04	2.67
Pr	1.12	0.02	0.01	1.32	0.01	0.01	0.02	0.01	1.01	0.02	4.24	0.01	0.04	0.03	0.02	0.01	0.02	0.03	0.07	0.03	0.14	0.14
Nd	4.09	0.08	0.10	5.07	0.06	0.05	0.10	0.19	4.07	0.09	18.93	0.15	0.27	0.15	0.14	0.13	0.15	0.22	0.41	0.18	1.66	1.74
Sm	0.90	0.04	0.04	1.22	0.03	0.02	0.07	0.05	0.80	0.04	2.22	0.07	0.13	0.07	0.07	0.07	0.08	0.09	0.17	0.10	2.20	1.79
Eu	2.46	<0.01	<0.01	3.15	<0.01	<0.01	<0.01	<0.01	2.20	<0.01	2.90	<0.01	<0.01	<0.01	<0.01	<0.01	<0.01	<0.01	<0.01	<0.01	0.30	0.28
Gd	0.96	0.16	0.29	1.19	0.23	0.18	0.25	0.28	0.87	0.15	2.34	0.20	0.35	0.20	0.23	0.19	0.32	0.20	0.39	0.28	8.81	6.84
Dy	0.51	0.50	1.00	0.90	0.84	0.55	0.63	0.73	0.76	0.61	1.28	0.34	0.66	0.49	0.43	0.54	0.62	0.56	0.63	0.72	28.38	26.40
Er	0.28	0.50	0.85	0.32	0.76	0.41	0.58	0.55	0.33	0.62	0.43	0.24	0.47	0.35	0.33	0.43	0.46	0.41	0.41	0.49	31.22	29.18
Yb	0.19	0.51	0.95	0.31	0.90	0.48	0.68	0.69	0.19	0.65	0.28	0.28	0.52	0.45	0.40	0.45	0.56	0.48	0.38	0.55	48.27	45.71
Lu	–	–	–	–	–	–	–	–	–	–	–	–	0.08	0.06	0.06	0.06	0.08	0.07	0.06	0.08	10.91	10.64
Zr/Hf	11	31	26	23	16	19	26	34	32	26	–	–	–	–	–	–	–	–	–	–	43	45
Y/Ho	–	–	–	–	–	–	–	–	–	–	–	–	–	–	–	–	–	–	–	–	26	27

Table 4
SIMS data on zircon from sample PBN 00-01

Spot #	U, ppm	Th, ppm	Pb, ppm	$^{206}Pb/^{204}Pb$, measured	$^{207}Pb/^{206}Pb$	$\pm\sigma$, %	$^{206}Pb/^{238}U$	$\pm\sigma$, %	$^{208}Pb/^{232}Th$	$\pm\sigma$, %	$^{206}Pb/^{238}U$ age, Ma	$\pm\sigma$	$^{208}Pb/^{232}Th$ age, Ma	$\pm\sigma$
01a	136	127	8	570	0.05955	2.8	0.04214	2.4	0.01298	4.7	266.1	6.3	260.8	12.1
01b	144	133	8	1834	0.05297	1.4	0.04205	2.4	0.01238	4.8	265.6	6.2	248.6	11.8
02c	124	121	7	1103	0.05214	1.7	0.03902	2.4	0.01291	4.7	246.8	5.8	259.3	12.0
02d	126	120	7	1957	0.05193	1.5	0.03993	2.4	0.01293	4.6	252.4	5.9	259.7	11.9
03e	110	135	6	773	0.05712	1.6	0.03495	2.4	0.01160	4.7	221.5	5.2	233.2	10.8
03f	113	137	6	1359	0.05321	1.8	0.03373	2.4	0.01129	4.7	213.8	5.0	226.9	10.6
04g	105	121	6	2146	0.05270	1.5	0.04080	2.4	0.01298	4.7	257.8	6.0	260.6	12.1

procedure is presented by Whitehouse and Platt (2003). The data are reported in Table 3.

3. Sample selection, petrography and mineral chemistry

Xenoliths are mostly fresh; they are angular or rounded and range in size from a few centimetres up to 10 cm. Mafic to ultramafic xenoliths selected for this study are collectively referred to as plutonic xenoliths. Pyroxenite xenoliths are commonly related to magmatic processes (Downes et al., 2001); on the contrary peridotitic xenoliths from Beaunit can be derived either from the residual (=metamorphic) mantle or from magmatic processes in the deep crust (granulitic facies). Plutonic ultramafic nodules display magmatic or sub-solidus textures and are commonly layered. They are distinguished from typical mantle-derived metamorphic xenoliths (Féménias et al., 2001) either by their textures, their mineral composition (lower $Mg^{\#}$ in the olivine down to 0.76; Fe^{3+}-rich spinels) or by the whole-rock chemistry (see discussion below and Fig. 3). Magmatic mafic nodules are distinguished from metamorphic sedimentary-derived crustal nodules by their higher whole-rock MgO content (Downes et al., 1990). All the plutonic ultramafic xenoliths show a typical macroscopic cumulative structure characterised by asymmetrical layering and by repetitive lithologic sequences.

3.1. Petrography

The ultramafic to mafic plutonic xenoliths from Beaunit are either homogeneous or finely layered. Major rock types are peridotites, pyroxenites and plagioclase-bearing rocks of gabbroic compositions.

All samples selected for detailed geochemical investigations are devoid of plagioclase but contain spinel (less than 2%). Their compositions range from peridotitic to pyroxenitic; they include dunite (PBN 98-54), harzburgite (PBN 98-13, PBN 98-27), lherzolite (PBN 86-24, PBN 98-05), olivine-websterite (PBN 98-09), orthopyroxene-rich websterite (PBN 86-19, PBN 98-39) and clinopyroxene-rich websterite (PBN 98-01). The grain size varies largely. Pyroxenites and plagioclase-bearing rocks show equigranular and polygonal textures. These textures and the lack of apparent zoning between core and rim of the silicate phases, as shown by detailed microprobe investigations, are typical features of sub-solidus recrystallised assemblages. Some ultramafic xenoliths nevertheless show heterogeneous grain-size distribution and incomplete thermodynamic equilibrium between silicate phases. These observations point to a partial sub-solidus recrystallisation of primary (=magmatic) assemblages. Orthopyroxene and olivine are the main cumulus phases, whereas clinopyroxene is frequently intergranular.

Accessory minerals are magnesio-hornblende (frequently observed in gabbroic rocks), Cr-spinel, Ti-rich phlogopite, apatite, ilmenite, rutile, pyrrhotite, pentlandite and srilankite ($(Zr,Ti)O_2$) (J. Jedwab, pers. commun.). They are included in the major silicate phases or are locally interstitial. Amphibole, phlogopite and coarse-grained oxides are in textural equilibria with the main silicate phases. The proportions of accessory minerals are strongly variable; they can be locally enriched in discrete layers by magmatic accumulation, as observed in some rare peridotite–chromitite layered samples.

Layered xenoliths are banded at millimetre to centimetre scale and include several peridotitic and pyroxenitic sequences. Mafic terms have gabbroic to anorthositic compositions. Several types of sequences have

been observed (Féménias et al., 2001), some of which have been investigated:

- websterite/lherzolite/harzburgite/lherzolite/dunite/lherzolite/websterite;
- websterite/lherzolite/olivine orthopyroxenite/websterite;
- plagioclase pyroxenite/anorthositic gabbro/websterite/gabbronorite;
- lherzolite/websterite/gabbro;
- gabbro/lherzolite/gabbro;
- olivine websterite/chromitite/olivine websterite/chromitite/lherzolite;
- norite/orthopyroxenite/norite (sample PBN 00-01);
- harzburgite/orthopyroxenite/norite/orthopyroxenite/norite (sample PBN 00-03).

Millimetre to centimetre scale layered xenoliths are not well suited for whole rock geochemical investigations. Consequently, two small ($8 \times 5 \times 5$ cm) well-layered samples have been selected for in-situ LA-ICP-MS and SIMS analyses of minerals. Sample PBN 00-01 is a plagioclase-bearing mafic–ultramafic layered xenolith, showing a millimetre scale norite–orthopyroxenite–norite succession. In detail, the orthopyroxenite layer is made of several sub-layers with variable grain-size and accessory mineral content. The coarser-grained orthopyroxenite sub-layer contains numerous accessory minerals including apatite, rutile, srilankite and a single zircon macrocryst. This suggests that this layer formed from a comparatively more differentiated magma. Sample PBN 00-03 is a composite mafic–ultramafic xenolith showing a rare harzburgite–orthopyroxenite–norite–orthopyroxenite–norite succession. These two samples underscore the intimate relationship between pyroxenite, peridotite and gabbro.

3.2. Mineral chemistry

Microprobe investigations were conducted mainly on ultramafic xenoliths. A few layered xenoliths were also analysed to characterise the mineralogical environment of the zircon-bearing layer (PBN 00-01). The magnesium contents of olivine, orthopyroxene, clinopyroxene and spinel, expressed as $Mg^{\#} = Mg/(Mg + Fe)$, calculated in cationic proportions, are reported in Fig. 2. Individual grains are homogeneous but in some

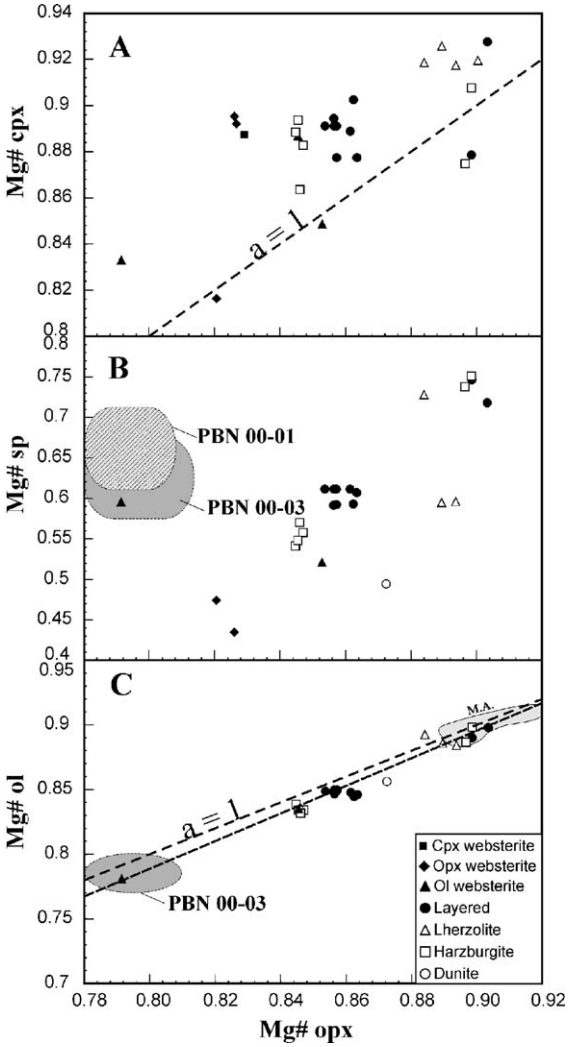


Fig. 2. Correlation between mineral compositions, expressed as $Mg^{\#} = Mg/(Mg + Fe)$ for orthopyroxene, clinopyroxene, spinel and olivine. Olivine and orthopyroxene compositions suggest equilibrium between the two phases, unlike for the ortho- and clinopyroxene pair (the line labelled a = 1 represents ideal equilibrium). The M.A. (Mantle Area) box represents the composition of mantle-derived xenoliths from Beaunit (Féménias et al., 2001). The boxes labelled PBN 00-01 and PBN 00-03 represent the compositional domains of the phases analysed by LA-ICP-MS.

cases, mineral phases show a range of composition for a given sample, as exemplified in Fig. 2 for samples PBN 00-01 and PBN 00-03. The $Mg^{\#}$ of the olivine is not correlated with the modal olivine content. The highest $Mg^{\#}$ ($Fo_{88.5-90}$) is observed in lherzolites, some harzburgites and some layered peridotites, while

the most common harzburgites and the dunite have lower $Mg^{\#}$ ($Fo_{83-85.5}$), close to those of the olivine-websterite layers present in layered pyroxenitic samples ($Fo_{84.5-85}$). The websterite with a very low olivine content has the lowest Fo content (Fo_{78}). Orthopyroxene has been observed in all petrographic types; its composition ranges from $Mg^{\#}=79$ to 90.5. The lherzolites, some harzburgites and layered peridotites have the highest $Mg^{\#}$ (88.5–90.5). The common harzburgites and dunite are less magnesian ($Mg^{\#}=84.5-87$). The websterites have the lowest $Mg^{\#}$ (79–85). The olivine and orthopyroxene compositions are nicely correlated (Fig. 2C), which suggests, in agreement with the petrographic observations, that they are in equilibrium. It is interesting to observe that olivine and orthopyroxene in the differentiated magmatic complex generally have compositions significantly more enriched in Fe than those of the mantle-derived xenoliths (Fig. 2C), although there is an overlap in the $Mg^{\#}$ range 88–92 for the pyroxene-rich lherzolites (Table 2)

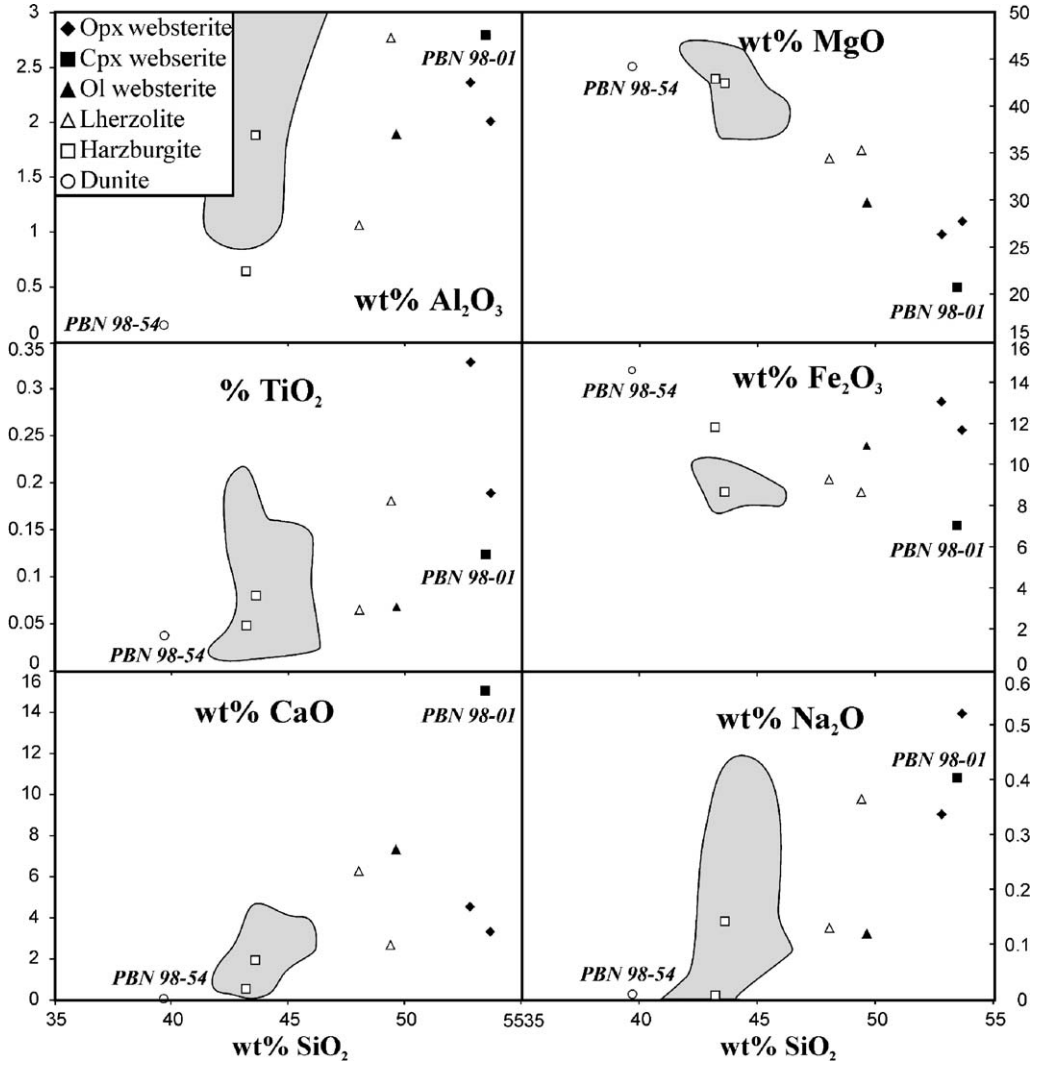


Fig. 3. Major element oxides vs. SiO_2 (in wt.%) for whole rock ultramafic xenoliths from Beaunit. PBN 98-54 is the most primitive dunite, PBN 98-01 is the most evolved sample with a high clinopyroxene content. For comparison, the field of mantle xenoliths (shaded domain) from the French Massif Central (Lenoir et al., 2000) has been reported.

and the harzburgite PBN 98-13 which is a thick horizon in a layered sample. The clinopyroxene is mainly a diopside that encompasses a large range of compositions ($Mg^{\#}$ = 81.5–92.5); it is poorly correlated with $Mg^{\#}$ of olivine and orthopyroxene (Fig. 2A). The orthopyroxene and olivine, in a single layered rock, show compositional variations that appear to be correlated with the modal proportion of the interstitial clinopyroxene. These relations observed for many layered samples cannot be interpreted by simple liquid–solid equilibria. They could possibly be related to a trapped liquid effect (Barnes, 1986) and a local sub-solidus equilibrium. The plagioclases are usually unzoned, except for the very thin overgrowths presumably due to the pyrometasomatic event (Faure et al., 2001). It displays a large range of compositions from An_{60} to An_{95}. The spinel belongs to the hercynite–chromite to spinel–magnesiochromite series ($Mg^{\#}$ = 0.45–0.75 and $Cr^{\#}$ = 0.15–0.7); locally it is enriched in Fe^{3+}, Fe^{2+} and Ti ($Fe^{3+\#}$ = 0.25 in opx-websterite), which suggests that it belongs to the "magmatic ore deposits domain" defined by Haggerty (1976) and not to the alpine type peridotites. Mg–Fe chromite is more common in dunite and in opx-rich websterite while the spinel in the websterites and peridotites is more aluminous. Spinel compositions are roughly correlated with orthopyroxene compositions (Fig. 2B).

4. Whole rock geochemical results on homogeneous xenoliths

Whole rock geochemical data have been obtained on representative homogeneous, monolithologic ultramafic xenoliths. The compositional range is quite large, and extends from 39.5 to 54 wt.% SiO_2 (Fig. 3). This range is much wider than the field of typical mantle-derived xenoliths from other occurrences of the French Massif Central (Lenoir et al., 2000). For Beaunit, MgO and SiO_2 are anti-correlated, while CaO and SiO_2 are roughly correlated; the compositional range directly reflects the variation in orthopyroxene, clinopyroxene and olivine modal contents. Accessory mineral modal abundance does not change the major element composition. The most evolved composition (sample PBN 98-01 with MgO = 20.9%) corresponds to a clinopyroxene-rich websterite that has high CaO (15%), Na_2O (0.41%) and Al_2O_3 (2.79%) contents. The least evolved composition is the dunite PBN 98-54 with 44.4% MgO and 39.7% SiO_2. The TiO_2, CaO Al_2O_3 and Na_2O contents are roughly correlated with SiO_2 and are related to the pyroxene content. The high total iron content of the Beaunit ultramafic xenoliths defines an Fe-rich series comparable to the ultramafic igneous or meta-igneous xenoliths from Bournac (Dupuy et al., 1979; Downes et al., 1990, 1991) and to classical mafic–ultramafic layered complexes (e.g. Bushveld: Eales and Cawthorn, 1996). The high Fe_2O_3tot whole rock content is consistent with the comparatively moderate $Mg^{\#}$ of the silicate phases. The near constant FeO*/MgO ratio with the marked SiO_2 increase (from 40 to 54 wt.%, Fig. 4) is typical of ultramafic cumulates formed during calc-alkaline magmatic differentiation (Miyashiro, 1974; Lachize et al., 1996).

The whole-rock chondrite-normalised REE abundances are given in Fig. 5. The clino- or orthopyroxene-rich websterites (Fig. 5A) have high REE contents (ΣREE: 9.2 to 19.7 ppm) with a typical LREE enrichment, $(La/Gd)_N$ ratios range from 3.5 to 5.3 and $(La/Yb)_N$ ratios from 3.8 to 7.2. Sample PBN 86-19 is

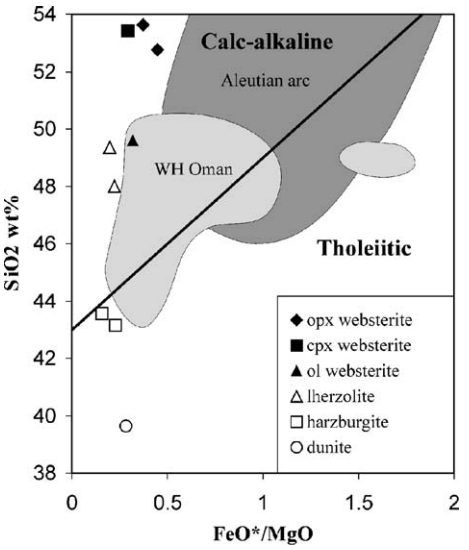


Fig. 4. SiO_2 vs. FeO*/MgO diagram (FeO* = FeO + Fe_2O_3) for whole rock compositions of the ultramafic magmatic xenoliths of Beaunit. The calc-alkaline–tholeiitic discriminant line is from Miyashiro (1974). The fields of calc-alkaline plutons from the Aleutian arc (compiled data from Kay et al., 1982) and Wadi Haymiliyah gabbros and norites (Lachize et al., 1996) are shown for comparison.

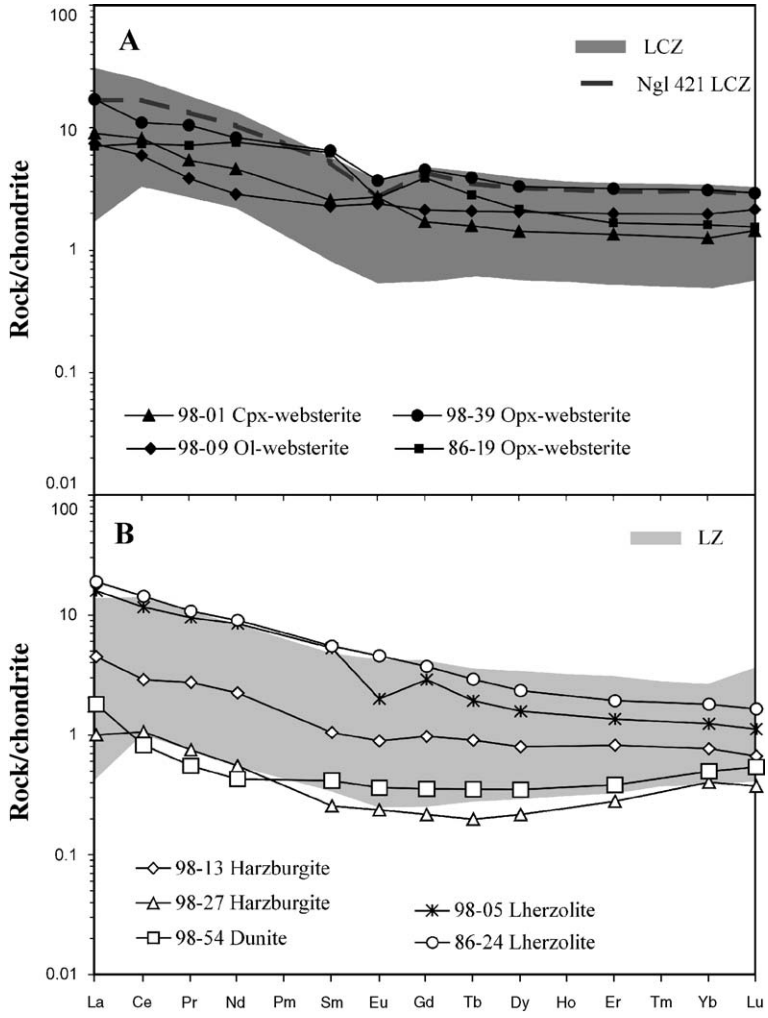


Fig. 5. Chondrite-normalised REE patterns for whole rock ultramafic xenoliths from Beaunit. Comparison with data from Lower Zone LZ (pyroxenite to dunite composition) and the Lower Central Zone LCZ of the Bushveld layered complex. Sample Ngl 421 is a typical orthopyroxenite from the LCZ of the Bushveld (data from Maier and Barnes, 1998). Normalising values from McDonough and Sun (1995).

distinguished by a flat LREE profile with $(La/Gd)_N$: 1.8. The pyroxene-rich lherzolites (Fig. 5B) have the highest REE contents (ΣREE = 17.8 and 21.3 ppm) and high $(La/Gd)_N$ (5.1 to 5.5) and $(La/Yb)_N$ (10.6 to 12) ratios; their profiles are similar to those of the websterites. The lherzolite PBN 98-05 and the two orthopyroxene-rich websterites (PBN 98-39 and PBN 86-19) display significant negative Eu anomalies (Eu/Eu* = 0.54 to 0.69) (Table 2). Comparable anomalies were observed by Downes and Dupuy (1987) on separated clinopyroxenes from a Beaunit nodule (Bt 36). Dunite and harzburgite samples (Fig. 5B) have the lowest REE content (ΣREE: 1.5 to 4.9 ppm) with LREE enriched patterns ($(La/Gd)_N$: 4.6 to 5.1; $(La/Yb)_N$: 2.5 to 5.9) and no significant Eu anomaly. The range of whole-rock REE contents is consistent with the interpretation that the xenoliths represent samples of a sequence of cumulates. They are indeed totally overlapping with the range of REE contents of two typical layered sequences of the Bushveld intrusion, the Lower Zone being dominated by peridotites (Fig. 5B) and the Lower Central Zone being dominated by

pyroxenites (data from Maier and Barnes, 1998). A typical orthopyroxenite (nlg 421) from this zone is given in Fig. 5A for comparison.

Multi-element diagrams normalised to pyrolite values (equivalent to the Primitive Mantle of McDonough and Sun, 1995) are shown in Fig. 6 for whole rock peridotites and websterites. Websterites and lherzolites are more enriched in trace elements than dunite and harzburgites. The spidergrams are all characterised by moderate but significant enrichments in all the large ion lithophile elements (LILE), Rb, Ba, Th, U and the LREE (3 to 10 times chondrites on average), relative to the high field strength elements (HFSE) Ta, Nb, Ti, Zr, Hf, Y and heavy rare earth elements (HREE) (usually less than the Pyrolite values). Most rocks (except the lherzolite PBN 98-24 and orthopyroxene-rich websterite PBN 98-39), exhibit more or less well pronounced negative Nb, Ta, and Ti anomalies. Trace element patterns of cumulate xenoliths from Beaunit are comparable to those observed in mantle xenoliths from the northern Massif Central (Lenoir et al., 2000). These anomalies are comparable to those measured in subduction-related magmatic series for which an upper mantle source metasomatised by fluids derived from

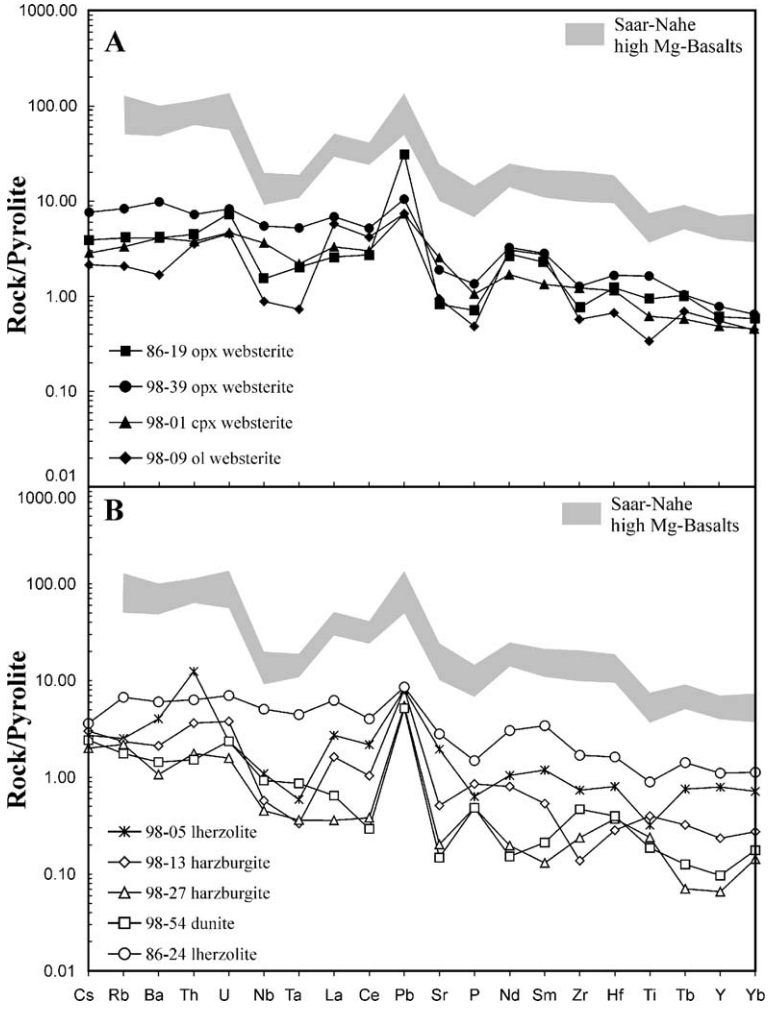


Fig. 6. Pyrolite-normalised multi-element variation diagrams for whole-rock ultramafic xenoliths from Beaunit. Comparison with Permian andesitic basalt from Saar–Nahe basin (data from Schmidberger and Hegner, 1999). Normalising values from McDonough and Sun (1995).

the subducting slab and selectively enriched in LILE is classically invoked (Pearce, 1983; McCulloch and Gamble, 1991; Scambelluri and Philippot, 2001).

5. LA-ICP-MS and SIMS investigation of layered xenoliths

5.1. REE and trace elements geochemical data on minerals

Trace element analyses were carried out by LA-ICP-MS on orthopyroxene and plagioclase from each sub-layer of layered samples PNB 00-01 and PNB 00-03. As clinopyroxene has a very low modal abundance (< 1%) and appears as tiny grains (< 50 μm), it has not been analysed by laser ablation. The chondrite-normalised REE patterns of orthopyroxene and plagioclase are given in Fig. 7. The profiles of orthopyroxene from the two samples are comparable, with rather low REE contents (ΣREE: 1.6 to 3.4 ppm) and LREE depletion: $(La/Yb)_N$ ratios range from 0.01 to 0.34 with $(Gd/Yb)_N$ in the range 0.34 to 0.83 for PBN 00-01 and 0.20 to 0.33 for PBN 00-03. Orthopyroxene grains close to the zircon macrocryst in sample PBN 00-01 (opx b, h and i; Fig. 7B) have slightly higher LREE contents (La_N: 0.36 to 0.68) than these close to the other grains (La_N: 0.09 to 0.36). All pyroxene analyses show a strong negative Eu

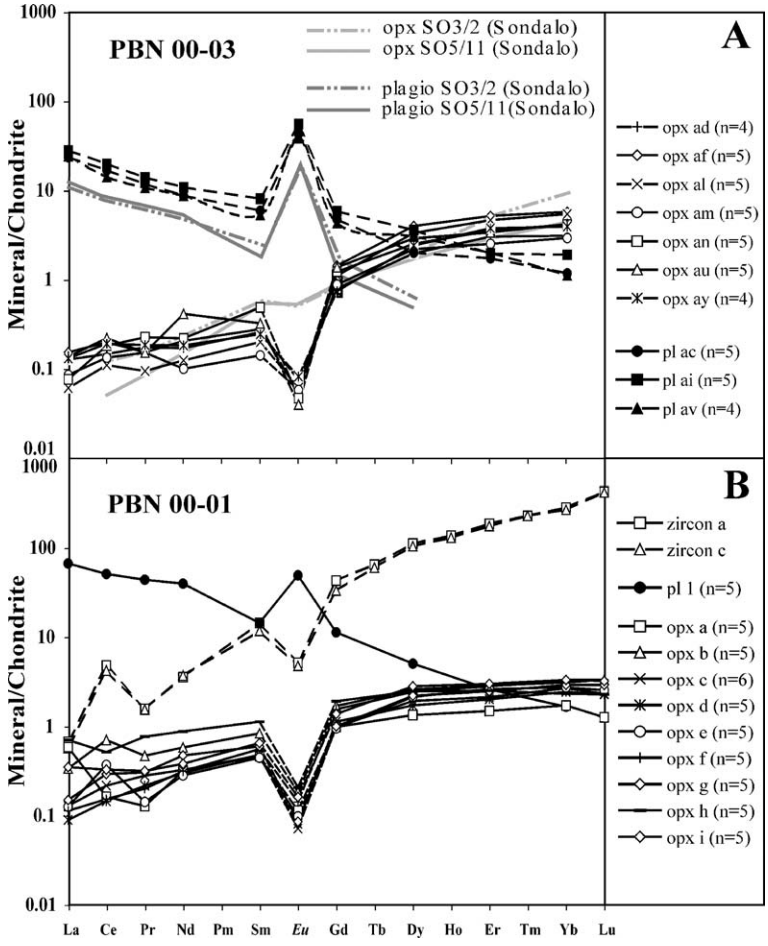


Fig. 7. Chondrite-normalised REE patterns for orthopyroxene and plagioclase (LA-ICP-MS) and zircon (SIMS) for two layered samples (PBN 00-01, which is zircon-bearing, and PBN 00-03). Each profile corresponds to the average of *n* measurements. For comparison, data obtained on the minerals of the Sondalo gabbroic complex (Tribuzio et al., 1999) have been reported. Normalising values from McDonough and Sun (1995).

anomaly (Eu/Eu* = 0.14 to 0.49) possibly enhanced by the poor precision on Eu measurements at such low level. There is no significant geochemical difference between the orthopyroxenes in adjacent millimetre-wide layers except for the Sr content that appears to be higher in orthopyroxene close to plagioclase-rich layers (opx ay, ad and af in Fig. 8). Pyrolite-normalised multi element diagrams (Fig. 8) show that the orthopyroxenes have low trace element abundances, especially for the most incompatible elements. They show Ta–Sr–LREE negative anomalies and relatively high Zr, Hf, HREE and Pb contents.

Four plagioclase grains have been analysed because they are the potential site for LREE location in these clinopyroxene-poor rocks. They appear to strongly control the whole rock signatures for many trace elements (LREE, Sr, Ba and Pb). In lherzolites and websterites, on the contrary, clinopyroxenes is the main carrier of these elements as shown by Downes and Dupuy (1987). The Beaunit plagioclases display strong LREE enrichments with $(La/Yb)_N$ ratios, in the range 15 to 20 for PBN 00-03 and 40 for PBN 00-01, strong positive Eu anomalies (Eu/Eu* = 3.9 to 8) and higher REE contents (ΣREE: 24.9 to 32.6 ppm for PBN 00-03 and 81.6 ppm for PBN 00-01) than in orthopyroxene. Trace elements patterns (Fig. 8) for three analysed plagioclases are characterised by a significant enrichment in LILE, Ba, LREE, Pb and Sr relative to the HFSE, Nb, Ta, Zr, Hf and Ti. So, plagioclase also exhibits to various degrees Nb, Ta and Ti negative anomalies.

The REE patterns observed in the orthopyroxenes and plagioclases of the Beaunit layered samples are in the same range of values as the minerals from the Sondalo gabbroic plutonic complex (Tribuzio et al., 1999), emplaced at the crust–mantle boundary during the Permian.

5.2. SIMS U–Th–Pb and trace elements analyses of zircon

The zircon crystal (1.5 mm in length) observed in sample PNB 00-01 is xenomorphic (Fig. 9). It is devoid of detectable zoning both under the optical microscope and scanning electron microscope in cathodoluminescence imaging mode. It contains fluid inclusions aligned along variably oriented surfaces and displays a few fractures filled with an undetermined mineral.

Seven U–Th–Pb isotopic analyses (Table 4) were performed in four pits in the crystal, avoiding fluid inclusions and fracture zones. Five analyses in three of

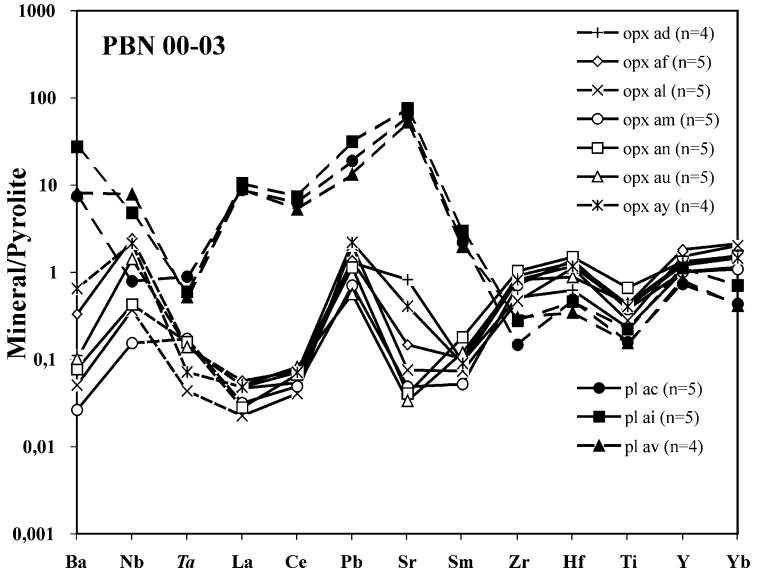


Fig. 8. Pyrolite-normalised multi-element variation diagrams for orthopyroxene and plagioclase (LA-ICP-MS) from the noritic layer of the layered sample PBN 00-03. Normalising values from McDonough and Sun (1995).

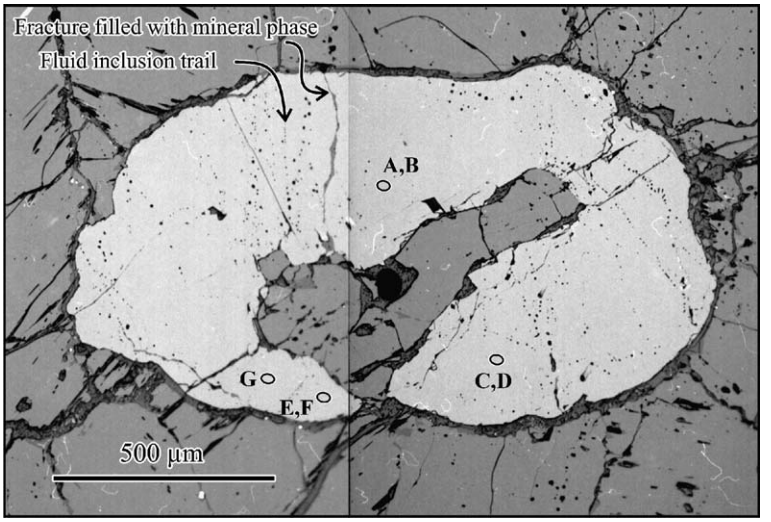


Fig. 9. Reflected-light photomicrograph of the zircon from the layered nodule PBN 00-01 with location of the SIMS U–Th–Pb geochronological investigation spots.

the pits are situated in the central part of the crystal (at more than 50 µm from the crystal edge). Four of them are concordant within analytical errors (analyses B, C, D, G), whereas the fifth (A) shows some surface contamination by common Pb possibly due to a microscopic inclusion or a surface crack (Fig. 10). The zircon is reasonably rich in U (100–150 ppm) and Th (120–140 ppm), and characterized by a Th/U ratio of 0.9 to 1.2. The five analyses yield an average $^{206}Pb/^{238}U$ age of 258 ± 9 Ma (weighted by errors on data points and a constant external error; MSWD = 1.9) and an equivalent average $^{208}Pb/^{232}Th$ age of 258 ± 11 Ma (weighted by errors on data points; MSWD = 0.2). The consistency of the results obtained with the $^{238}U-^{206}Pb$ and $^{232}Th-^{208}Pb$ decay systems is a very good indication that the age reflects the crystallisation of the zircon. Regression of the five data points, anchored with common Pb of modern composition, yields an intercept age of 257 ± 6 Ma (MSWD = 1.6), regarded as the best estimate for the crystallisation age. This age corresponds to the Permian period (295–250 Ma, following the IUGS International Stratigraphic Chart). Two analyses (03e, 03f), in one pit situated at 40 µm from the edge of the crystal, are discordant and yield younger $^{206}Pb/^{238}U$ ages. This trend suggests surface Pb loss, possibly linked to Quaternary pyrometamorphism.

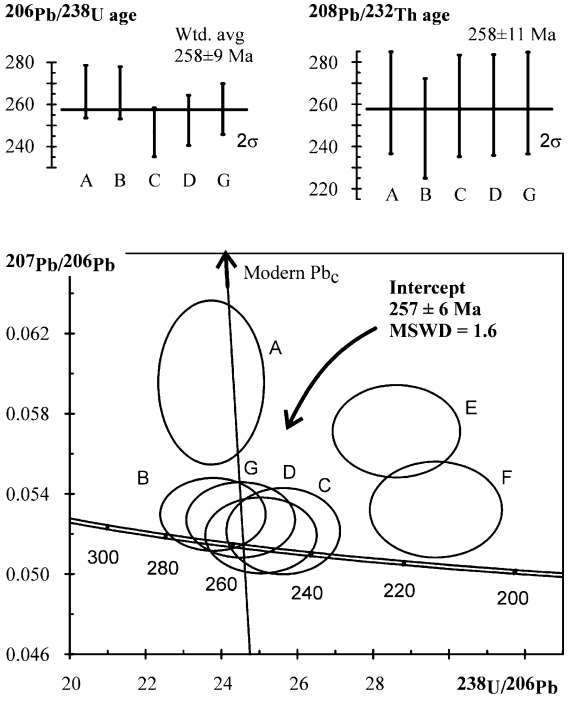


Fig. 10. SIMS U–Th–Pb geochronological data on the zircon from the layered nodule PBN 00-01. The best estimated crystallisation age is 257 ± 6 Ma, calculated with the Isoplot program (Ludwig, 1999).

Trace element analyses of REE, Y and Hf, were carried out in two of the pits (A,B and C,D on Fig. 9) left after Th–U–Pb analyses. The zircon displays a HREE-enriched pattern with a Lu_N value of 440, a very low $(La/Yb)_N$ ratio of 0.002, a positive Ce anomaly and a negative Eu anomaly ($Eu/Eu^* = 0.21–0.24$). The zircon has a Zr/Hf ratio of 43–45, slightly higher than the chondritic value of 38, and a chondritic Y/Ho ratio of 26–27.

Zircon in crustal magmatic and metamorphic rocks has a fairly homogeneous trace-element signature characterised by HREE enrichment ($10^2 < Lu_N < 10^4$), a negative Eu anomaly and a positive Ce anomaly (Hoskin and Ireland, 2000; Rubatto, 2002). Zircon in metamorphic rocks has a low Th/U ratio (< 0.1) and can display variations in HREE or MREE signatures depending on metamorphic assemblages (Rubatto, 2002; Whitehouse and Platt, 2003). Zircon from kimberlites, carbonatites and mantle-derived nodules recovered from kimberlites have a specific trace element signature characterized by the absence of Eu anomalies and low abundance in HREEs and Y ($10 < Lu_N < 100$; Dawson et al., 2001; Belousova et al., 1998). The trace element content of the zircon of sample PNB 00-01 is typical for a magmatic crustal rock. The negative Eu anomalies of the zircon and associated orthopyroxene can be directly related to the strong positive anomalies of the associated plagioclase. This is a fairly common feature in many igneous zircons and reflects the ubiquity of plagioclase in zircon crystallising environments.

6. Discussion

6.1. Parental magma and crystallisation history

The population of plutonic xenoliths found in the Beaunit scoria comprises samples without and with well-developed layering, which display a large lithological variety ranging from ultramafic (lherzolite, pyroxenite) to mafic (gabbro, gabbronorite, plagioclase-rich anorthositic gabbro) horizons. Petrographic observations, mineral chemistry (orthopyroxene, plagioclase) and geochemical data obtained both on whole rock for unlayered samples and on minerals for layered nodules suggest that the two types of nodules could be derived from a single layered intrusion. The whole rock trace element patterns, particularly the REE patterns, of the suite of plutonic xenoliths are comparable to those observed in ultramafic cumulates of layered intrusions, as exemplified by the rocks from the Lower Zone and Lower Central Zone of the Bushveld complex (Maier and Barnes, 1998) (Fig. 5). Trace element and REE concentrations in a sequence of cumulates are largely governed by the position of the different samples in the stratigraphic column and by the relative amounts of cumulus phases and inter-cumulus material (= interstitial trapped liquid). In randomly sampled nodules found in lava, the structural correlation between different xenoliths is obviously not known, moreover the sub-solidus re-equilibration textures tend to blur the primary (= magmatic) textures. Nevertheless, the quite high incompatible trace element contents in the pyroxenites and lherzolites of Beaunit suggest a high proportion of post-cumulus liquid; these rocks probably displayed meso- to ortho-cumulate textures originally. On the contrary, dunite and harzburgites have significantly lower incompatible trace element contents; they presumably had an adcumulate texture.

The plagioclases of the layered nodules (analysed by LA-ICP-MS) have typical positive Eu anomalies while negative Eu anomalies are observed in some unlayered pyroxenites and lherzolites, as well as in separated orthopyroxene and zircon from layered rocks. This confirms that the REE patterns of whole rocks are largely controlled by the mineralogical composition of the cumulates; this again implies that a cumulation process has been an important phenomenon. Our data suggest that the pyroxenites represent differentiated cumulates (as previously proposed by Downes and Dupuy, 1987), some of them with quite low orthopyroxene $Mg^{\#}$ being formed from a residual liquid left after plagioclase fractionation. It has been shown experimentally (Müntener et al., 2001) that low H_2O content (< 3%) in the magma stabilises plagioclase earlier than amphibole, this could also explain the low proportion of hydrated phases. From the petrography and mineral chemistry, it can be assumed that olivine and orthopyroxene were the first fractionating phases generating dunitic and harzburgitic cumulates. This suggests that the parental magma might be a high-Mg basalt. Plagioclase and clinopyroxene first crystallised as intercumulus phases from the trapped liquid. Later they fractionated as cumulates

forming gabbros and plagioclase-rich rocks. The negative Eu anomalies observed in the most differentiated pyroxenites imply that they were formed after plagioclase fractionation.

Even if the distribution of some trace elements is partially controlled by the mineralogical composition of the rocks, other geochemical features such as the enrichment in LILE and LREE relative to Nb, Ta and Ti can be interpreted as signature of the parental magma. Beaunit cumulates have geochemical signatures quite comparable to the trace elements patterns of the subcontemporary Permo-Carboniferous magmatism (Benek et al., 1996), more particularly of the Saar–Nahe–Lorraine basalts (Fig. 6; data from Schmidberger and Hegner, 1999) and of the subduction-related Alpine and Sardinian magmatism (Cortesogno et al., 1998). The plutonic mafic nodules from Beaunit also show some similarity, both on the textural and mineralogical aspects, to the ''meta-igneous'' nodules found in the Bournac pipe (Leyreloup et al., 1977; Dostal et al., 1980; Downes and Leyreloup, 1986; Downes et al., 1990). Other mafic, and more rarely ultramafic, xenolith occurrences of the French Massif Central have been interpreted as cumulates of calc-alkaline affinity (Downes and Leyreloup, 1986; Downes et al., 1990). We suggest that the Beaunit layered complex could belong to this magmatic suite. It thus appears that several plutons of calc-alkaline affinity have been underplated beneath the Massif Central during the Permo-Carboniferous period. This event has a wide regional significance.

6.2. Emplacement age of the deep layered intrusion

Zircon has been found in one layered plutonic xenolith from puy Beaunit (sample PBN 00-01). The rock presents all the features of an undeformed igneous layered sample with a norite–orthopyroxenite–norite succession that has been observed in other xenoliths. The zircon macrocryst has a trace element signature typical for zircon formed in a magmatic environment. The negative Eu anomaly in zircon coupled to the anomalies in the associated orthopyroxene (negative anomaly) and plagioclase (positive anomaly) strongly suggests a cogenetic origin for these minerals that most probably derived from the same liquid. This unique zircon-bearing layered nodule probably belongs to the same cumulate sequence, as the other plagioclase- and orthopyroxene-rich layered samples. This crystal could be the very late crystallising phase in a highly evolved, SiO_2-saturated, trapped interstitial melt. The xenomorphic shape of the zircon, the lack of visible internal zoning and the occurrence of fluid inclusions in apparently randomly oriented planes indicate that the observed crystal is not a direct product of magmatic crystallisation (in that case, it would have developed a prismatic habit with crystal faces). It was probably affected by sub-solidus secondary recrystallisation, during which the original zoning pattern was homogenised and grain boundary migration occurred. This process probably took place during cooling of the magmatic body. The present-day composition of the core of the crystal and the age record probably reflect this sub-solidus secondary recrystallisation. The SIMS age obtained, 257 ± 6 Ma, can be interpreted either as the magmatic crystallisation age of the zircon or as the subsolidus cooling age under closed system granulite facies conditions, each mineral phase keeping its REE magmatic signature. It nevertheless allows the deep layered intrusion beneath Puy Beaunit to be related to a Permian context of emplacement.

The age of the abundant lower crustal xenoliths collected in the Massif Central is poorly constrained. The depositional or stratigraphic age of the metasedimentary granulites has been considered to be Late Proterozoic (Downes et al., 1991). Both metasedimentary and felsic meta-igneous granulitic xenoliths from Bournac contain zircons and monazites with U–Pb ages in the range 250–310 Ma (Supply, 1981 discussed in Downes et al., 1991 and in Costa and Rey, 1995). The 257 ± 6 Ma age obtained for the Beaunit layered intrusion falls in this range of ages. Sm–Nd and Rb–Sr systematics on crustal xenoliths from Bournac do not give any isochron relationships: Downes et al. (1990) have suggested that the data result from the mixing between mantle-derived mafic magmas of late-Variscan age, and pre-existing (metasedimentary) crustal material.

6.3. Late- to post-Variscan geotectonic setting of the layered intrusion

The plutonic xenoliths found in the Beaunit scoria cone most probably come from a differentiated, deep layered intrusion emplaced during the Permian, at or slightly before 257 ± 6 Ma. This magmatic event is

late- to post-Variscan in age, and can be related to a calc-alkaline late- to post-orogenic episode. After major thickening and post-orogenic collapse, the late-Variscan period is characterised by a widespread episode of fracturing that affects not only the Variscan fold-belt itself but also its neighbouring platforms, from Northern Africa to Northeastern Europe (Arthaud and Matte, 1975). This tectonic event was younger than the main Variscan tectonogenesis. In the French Massif Central area, it corresponds to the end of the main crustal deformation event (Chen et al., 1997). It resulted in the formation of wrench-faults related to a N–S to NW–SE compression (Arthaud and Matte, 1975), interpreted as the final continental collision of Gondwana with the Appalachian–Variscan fold-belt (Prost and Becq-Giraudon, 1989). Transcurrent basin tectonics, characterised by the development of pull-apart structures (Mattauer and Matte, 1998), occurred during the Late Carboniferous to Early Permian; several Late-Paleozoic basins with half-graben structure were opened (Arthaud and Matte, 1975; Faure, 1995; Chen et al., 1997). Although the dynamic conditions of this basin opening are not settled, an extensional setting appears likely. Related to local transtensional context, the Massif Central Permian basins are in fact transcurrent to the major N–S direction of the tectonic accident of the "Sillon Houiller". Mafic magma emplacement occurred during this event, from the Oslo Graben in the north to Italy and northern Africa in the south (Matte, 1991; Doblas et al., 1998). Several magmatic complexes have been described in the Northeast German basin (Benek et al., 1996), in Scotland (Downes et al., 2001), in Saar–Nahe (Schmidberger and Hegner, 1999), in the Pyrenees (Innocent et al., 1994), Corsica (Cabanis et al., 1990), Ligurian Alps, Southern Alps and Sardinia (Cortesogno et al., 1998) and northern French Massif Central (Collomb and Feys, 1964). The magmatic activity was not restricted to high-level, volcanic to sub-volcanic events; several deep-seated complexes have been inferred from geophysical investigations (DEKORP-BASIN Res. Group, 1999) or are exposed as a result of Alpine tectonism and exhumation (Voshage et al., 1990; Tribuzio et al., 1999; Hermann et al., 2001). These permo-carboniferous magmatic occurrences have been variously interpreted in terms of mode of emplacement and relation with the local tectonics. This magmatic activity has been related to a crustal thinning by many authors (see above). On the contrary, Costa and Rey (1995) suggest that comparable mantle-derived mafic magma emplaced in the lower crust during the major thickening event. In that respect, the layered intrusion of Beaunit is interesting because this area is a rare exclusively intracontinental occurrence. Tectonomagmatic activity during the Permian can be summarised as transcurrent basin tectonics at the surface, associated with crustal thinning and regional upwelling of the shallow lithosphere. The Beaunit area is located in the southwestern extension of the Le Creusot–Blanzy Permian basin (actually masked by Cenozoic volcanoes and the Tertiary Limagne Basin; Fig. 1B) in which volcanic activity has been described (Collomb and Feys, 1964). This Upper Paleozoic graben, bounded by 100-km-long complex transform faults, was predominantly controlled by a trans-tensional tectonic regime (Golitsyn et al., 1997). Neither subduction nor back-arc volcanism can be invoked to explain the sub-alkaline affinity of the Beaunit deep complex which occurred ca. 100 Ma after continent–continent collision, during the Late Permian in such an intracontinental setting.

6.4. Melt generation and mantle source

In the northern part of the French Massif Central, several Palaeozoic terranes, assigned to the Moldanubian Zone (Pharaoh, 1999), were integrated into Europe's mosaic of terranes by a complex Variscan history (Fig. 1A). The Massif Central itself results from a major collage between a southern terrane and a northern Moldanubian terrane, related to Gondwana (Meissner, 1999). In the Massif Central and South Armorica, the presence of ophiolites, oceanic materials and volcanic arcs indicates a Late Devonian active margin. One of the major thrust sutures related to plate convergence has been identified, north of the present-day Beaunit area, from which calc-alkaline subduction-related materials have recently been described (Pin and Paquette, 2002). South of the Beaunit area, a mantle suture has also been proposed by Lenoir et al. (2000) on the basis of regional geochemical investigations on peridotite xenoliths. They proposed that this suture is sub-parallel to one of the major boundaries described by Matte (1986). Whatever the tectonic model, the Beaunit area is located above a subduction zone dipping either to the north (Matte, 1986) or to the

south (Pin and Paquette, 2002). It is suggested that the subcontinental mantle wedge above the subduction zone has been modified by metasomatic hydrous fluids derived from dehydration and/or melting of the subducting slab as described in active subduction zones (Vidal et al., 1989; Defant and Drummond, 1990; Maury et al., 1992; Prouteau et al., 1999). Mantle nodules sampled by Cainozoic volcanoes in the northern part of the Massif Central (Lenoir et al., 2000) show enriched trace element patterns that probably derived from such a metasomatic mantle.

The enrichment in LILE and LREE elements, relative to Nb, Ta and Ti, observed in late- to post-orogenic calc-alkaline magma series can be explained by several mechanisms (e.g. Aldanmaz et al., 2000): (i) inheritance of a subduction component derived from an earlier subduction event, (ii) crustal contamination through assimilation and fractional crystallisation (AFC process; De Paolo, 1981) and (iii) a melting, assimilation, storage and homogenisation (MASH) process. It has been shown by isotopic data (Pin and Sills, 1986; Voshage et al., 1990; Downes et al., 1990) that several late-Variscan ultramafic–mafic intrusions, comparable to the Beaunit deep complex, have been contaminated by bulk crustal assimilation and/or a combined assimilation and fractional crystallisation mechanism. The sub-alkaline basaltic parental magma has assimilated the metasedimentary granulitic country rocks. These studies show that the ultramafic cumulates and the peridotites are generally the least contaminated rocks, the mafic cumulates (gabbros) being more contaminated. If the metasedimentary granulitic xenoliths found in the Cainozoic volcanoes (Leyreloup, 1974; Leyreloup et al., 1977; Dostal et al., 1980) do effectively represent the local deep crust in the Massif Central, their compositions are not suitable to explain the general trace element patterns and enrichment of the ultramafic part of the Beaunit plutonic complex. The mafic plutonic nodules from Beaunit could be compared to the meta-igneous granulites and mafic nodules found in the Bournac and Roche Pointue lavas. For the latter, Downes and Leyreloup (1986) and Downes et al. (1990) have suggested that they represent cumulates derived from mafic calc-alkaline to tholeiitic liquid contaminated by continental crust as shown by the Sr–Nd isotopic composition.

All the Permian deep intrusions identified so far have been considered to result from the crystallisation and differentiation of a mantle-derived mafic magma. The two likely mechanisms for magma generation are thus: (1) melting of lithospheric mantle by adiabatic decompression resulting from lithospheric extension or uplift; (2) melting of lithospheric mantle by perturbation of the local geotherm by heat from an upwelling asthenospheric mantle, which could be generated by lithospheric delamination or by detachment of the subducted slab. The post-collisional history of the Variscan fold-belt is difficult to reconcile with an important lower crustal deformation, delamination or slab detachment during the Permian. Nevertheless, the transcurrent regime deduced from the observation of surface structures argues for a local uplift of the lithospheric mantle linked to the development of pull-apart basins in the crust. Partial melting of the upper mantle possibly took place during this event. The validity of this mechanism depends largely on the existence of hydrous conditions in the mantle to produce melt. As the enrichment in LILE and LREE elements relative to Nb, Ta and Ti observed in calc-alkaline suites is generally ascribed to a mantle source that has been metasomatically enriched by subduction-related hydrous fluids/liquids (Pearce, 1983; McCulloch and Gamble, 1991; Scambelluri and Philippot, 2001), we suggest that the trace element signature observed in the Beaunit ultramafic xenoliths also implies such a metasomatically enriched mantle source, in agreement with the chemical features of the mantle xenoliths of the northern part of the French Massif Central (Lenoir et al., 2000).

7. Conclusions

Mafic and ultramafic plutonic xenoliths from Beaunit scoria cone presumably derive from a differentiated, deep layered intrusion in which fractional crystallisation, mineral cumulation and substantial sub-solidus recrystallisation occurred. The 257 ± 6 Ma zircon U–Pb age indicates that the intrusion formed by mafic underplating during Permian time. The geotectonic context of the area and the calc-alkaline geochemical signature suggests that the formation of the Beaunit layered intrusion occurred in two steps (Fig. 11):

(i) a Late Devonian (370–360 Ma) enrichment event occurred in the mantle after the subduction

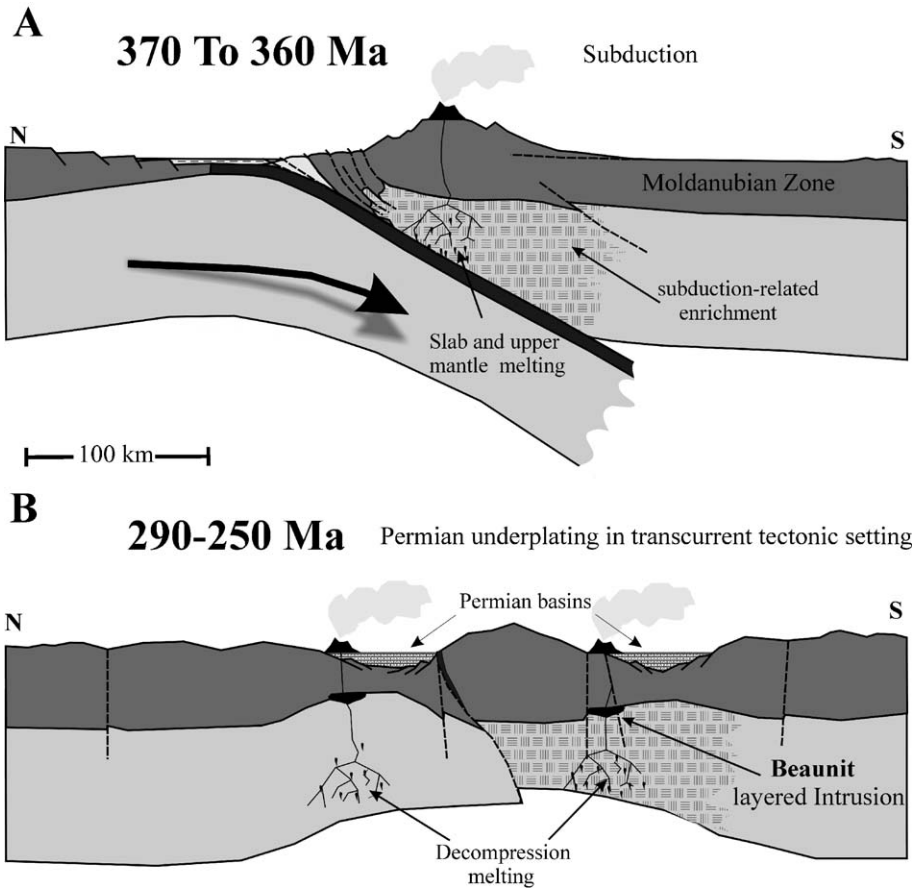


Fig. 11. Hypothetic schematic sections across the "Northern French Massif Central". (A) S-dipping paleo-ocean subduction and contemporary mantle enrichment (370–360 Ma), after Pin and Paquette (2002). (B) Permian crustal thinning, transcurrent basin tectonics and lithospheric uplift during emplacement of the Beaunit deep layered intrusion.

(Pin and Paquette, 2002) beneath the Moldanubian zone and the Ibero–Gondwana terranes that constituted the southern part of the Variscan domain. This metasomatic, subduction-related event introduced a hydrous (and magmatic?) component enriched in LILE and LREE relative to Nb, Ta and Ti. This enriched mantle source will have a considerable importance for the next upper mantle melting episode.

(ii) a Late-Variscan (290–250 Ma) intracontinental magmatic episode took place in relation with late- to post-orogenic basin tectonics in intracontinental position. This magmatism is characterised by a calc-alkaline geochemical affinity, as observed in the Beaunit xenoliths and in other regional xenolith occurrences (i.e. Bournac: Downes and Leyreloup, 1986; Downes et al., 1990). During the Permian, the magmatic manifestations are related to late- or post-orogenic basin tectonics, and occurred along major crustal structures. Beaunit is located at the possible southwestern extension of the Blanzy–Le Creusot Permian basin.

Acknowledgements

J. Jedwab is thanked for the "discovery" of the zircon in one of our samples. Comments by C. Pin on a preliminary version of this paper helped us clarify our understanding of the Variscan evolution of the

French Massif Central. The constructive and thorough reviews of X. Lenoir and H.G. Stosch are gratefully acknowledged. The suggestions of R. Rudnick (Editor of Chemical Geology) were also helpful.

The Nordsim facility is funded by the Research Funding Agencies of Denmark, Finland, Norway and Sweden together with the Swedish Museum of Natural History (Stockholm, Sweden). We thank K. Högdahl and T. Sunde for technical assistance. **[RR]**

References

Aldanmaz, E., Pearce, J.A., Thirlwall, M.F., Mitchell, J.G., 2000. Petrogenetic evolution of late Cenozoic, post-collision volcanism in western Anatolia, Turkey. J. Volcanol. Geotherm. Res. 102, 67–95.

Arthaud, F., Matte, P., 1975. Les décrochements tardi-hercyniens du sud-ouest de l'Europe. Géométrie et essai de reconstitution des conditions de la déformation. Tectonophysics 25, 139–171.

Barnes, S.J., 1986. The effect of trapped liquid crystallisation on cumulus mineral compositions in layered intrusions. Contrib. Mineral. Petrol. 93, 524–531.

Belousova, E.A., Griffin, W.L., Pearson, N.J., 1998. Trace element composition and cathodoluminescence properties of southern African kimberlitic zircons. Mineral. Mag. 62, 355–366.

Benek, R., Kramer, W., McCann, T., Scheck, M., Negendank, J.F.W., Korich, D., Huebscher, H.-D., Bayer, U., 1996. Permo-Carboniferous magmatism of the Northeast German Basin. Tectonophysics 266, 379–404.

Brousse, R., Rudel, A., 1964. Bombes de péridotites, de norites, de charnockites et de granulites dans les scories du puy Beaunit. C. R. Acad. Sci. Paris 259, 185–188.

Cabanis, B., Cochemé, J.J., Vellutini, P.J., Joron, J.L., Treuil, M., 1990. Post-collisional Permian volcanism in northwestern Corsica: an assessment based on mineralogy and trace-element geochemistry. J. Volcanol. Geotherm. Res. 44, 51–67.

Chantraine, J., Autran, A., Cavelier, C., Alabouvette, B., Barféty, J.-C., Cecca, F., Clozier, L., Bertrand-Passard, S., Dubreuilh, J., Feybesse, J.-L., Guennoc, P., Ledru, P., Rossi, P., Ternet, Y., 1996. Carte géologique de la France à 1/1000000, BRGM Service géologique national, Orléans.

Chen, Y., Faure, M., Cogné, J.P., 1997. Late Permian paleomagnetic results from the Brive basin (Massif Central, France). Tectonophysics 281, 209–220.

Collomb, P., Feys, R., 1964. Manifestations éruptives dans l'Autunien de Blanzy-Creusot (Saône-et-Loire). C. R. Acad. Sci. Paris 258 (24), 5915–5917.

Cortesogno, L., Cassinis, G., Dallagiovanna, G., Gaggero, L., Oggiano, G., Ronchi, A., Seno, S., Vanossi, M., 1998. The Variscan post-collisional volcanism in Late Carboniferous–Permian sequences of Ligurian Alps, Southern Alps and Sardinia (Italy): a synthesis. Lithos 45, 305–328.

Costa, S., Rey, P., 1995. Lower crustal rejuvenation and growth during post-thickening collapse: insights from a crustal cross section through a Variscan metamorphic core complex. Geology 23, 905–908.

Dawson, J.B., Hill, P.G., Kinny, P.D., 2001. Mineral chemistry of a zircon-bearing, composite, veined and metasomatised upper-mantle peridotite xenolith from kimberlite. Contrib. Mineral. Petrol. 140, 720–733.

Defant, M.J., Drummond, M.S., 1990. Derivation of some modern arc magmas by melting of young subducted lithosphere. Nature 347, 662–665.

DEKORP-BASIN Res. Group, 1999. Deep crustal structure of the Northeast German basin: neo DEKORP-BASIN '96 deep-profiling results. Pure Appl. Geophys. 27, 55–58.

De Paolo, D.J., 1981. Trace element and isotopic effects of combined wallrock assimilation and fractional crystallisation. Earth Planet. Sci. Lett. 53, 189–202.

Doblas, M., Oyarzun, R., Lopez-Ruiz, J., Cebria, J.M., Youbi, N., Mahecha, V., Lago, M., Pocovi, A., Cabanis, B., 1998. Permo-Carboniferous volcanism in Europe and northwest Africa: a superplume exhaust valve in the centre of Pangea? J. Afr. Earth Sci. 26 (1), 89–99.

Dostal, J., Dupuy, C., Leyreloup, A.F., 1980. Geochemistry and Petrology of Meta-igneous granulitic xenoliths in Neogene volcanic rocks of the Massif Central, France—implication for the lower crust. Earth Planet. Sci. Lett. 50, 31–40.

Downes, H., Dupuy, C., 1987. Textural, isotopic and REE variations in spinel peridotite xenoliths, Massif Central, France. Earth Planet. Sci. Lett. 82, 121–135.

Downes, H., Leyreloup, A.F., 1986. Granulitic xenoliths from the French Massif Central-petrology, Sr and Nd isotope systematics and model age estimates. In: Dawson, J.B., Hall, J., Carswell, D.A., Wedepohl, K.H. (Eds.), The nature of the lower continental crust. Geol. Soc. London, Spec. Publ., vol. 24, pp. 319–330.

Downes, H., Dupuy, C., Leyreloup, A.F., 1990. Crustal evolution of the Hercynian belt of Western Europe: evidence from lower-crustal granulitic xenoliths (French Massif Central). Chem. Geol. 83, 209–231.

Downes, H., Kempton, P.D., Briot, D., Harmon, R.S., Leyreloup, A.F., 1991. Pb and O isotope systematics in granulite facies xenoliths, French Massif Central: implications for crustal processes. Earth Planet. Sci. Lett. 102, 342–357.

Downes, H., Upton, B.G.J., Handisyde, E., Thirlwall, M.F., 2001. Geochemistry of mafic and ultramafic xenoliths from Fidra (Southern Uplands, Scotland): implications for the lithospheric processes in Permo-Carboniferous times. Lithos 58, 105–124.

Dupuy, C., Leyreloup, A.F., Vernières, J., 1979. The lower continental crust of the Massif Central (Bournac, France) with special references to REE, U and Th composition, evolution, heat flow production. In: Ahrens, L.H. (Ed.), Origin and Distribution of the Elements. Pergamon, Oxford, pp. 401–415.

Eales, H.V., Cawthorn, R.G., 1996. The Bushveld complex. In: Cawthorn, R.G. (Ed.), Layered Intrusions. Elsevier, Amsterdam, pp. 181–229.

Faure, M., 1995. Late orogenic Carboniferous extensions in the Variscan French Massif Central. Tectonics 14, 132–153.

Faure, F., Trolliard, G., Montel, J.-M., Nicollet, C., 2001. Nano-

petrographic investigation of a mafic xenolith (maar de Beaunit, Massif Central, France). Eur. J. Mineral. 13, 27–40.

Féménias, O., Mercier, J.-C.C., Demaiffe, D., 2001. Petrology of ultramafic xenoliths from the Puy Beaunit (French Massif Central): an unusual occurrence for the sub-continental mantle. C. R. Acad. Sci. Paris IIA 332, 535–542.

Goër de Herve, A., Boivin, P., Camus, G., Gourgaud, A., Kieffer, G., Mergoil, J., Vincent, P., 1991. Volcanologie de la chaîne des Puys, Parc Naturel Régional des Volcans d'Auvergne. Imp. Moderne ed., Aurillac. 127 pp.

Golitsyn, A., Courel, L., Debriette, P., 1997. A fault-related coalification anomaly in the Blanzy–Montceau Coal Basin (Massif Central, France). Int. J. Coal Geol. 33, 209–228.

Govindaraju, K., 1994. Compilation of working values and samples description for 383 geostandards. Geostand. Newsl. 15, 139–143.

Haggerty, S.E., 1976. Opaque mineral oxides in terrestrial igneous rocks. In: Rumble, D. (Ed.), Oxide Minerals. Min. Soc. Am., Short Course Notes, vol. 3, pp. 101–300.

Hermann, J., Müntener, O., Günther, D., 2001. Differentiation of mafic magma in a continental crust-to-mantle transition zone. J. Petrol. 42 (1), 189–206.

Hoskin, P.W.O., Ireland, T.R., 2000. Rare earth element chemistry of zircon and its use as a provenance indicator. Geology 28, 627–630.

Innocent, C., Briqueu, L., Cabanis, B., 1994. Sr–Nd isotope and trace element geochemistry of late Variscan volcanism in the Pyrenees: magmatism in post-orogenic extension? Tectonophysics 238, 161–181.

Jarvis, K.E., 1990. A critical evaluation of two sample preparation techniques for low-level determination of some geologically incompatible elements by inductively coupled plasma-mass spectrometry. Chem. Geol. 83, 89–103.

Kay, S., Kay, R.W., Citron, G.P., 1982. Tectonic controls on Aleutian tholeiitic and calc-alcaline magmatism. J. Geophys. Res. 87, 4051–4072.

Lachize, M., Lorand, J.P., Juteau, T., 1996. Calc-alkaline differentiation trend in the plutonic sequence of the Wadi Haymiliyah section, Haylayn massif, Semail ophiolite, Oman. Lithos 38, 207–232.

Le Maitre, R.W., 1989. A classification of igneous rocks and glossary of terms. Recommendations of the International Union of Geological Sciences Subcommission on the Systematics of Igneous Rocks. Blackwell, Oxford. 193 pp.

Lenoir, X., Garrigo, C.J., Bodinier, J.-L., Dautria, J.-M., 2000. Contrasting lithospheric mantle domains beneath the Massif Central (France) revealed by geochemistry of peridotite xenoliths. Earth Planet. Sci. Lett. 181, 359–375.

Leyreloup, A.F., 1973. Le socle profond en Velay d'après les enclaves remontées par les volcans néogènes, son thermométamorphisme et sa lithologie: granites et série charnockitique (Massif Central français). Thèse 3ème cycle, Univ. Nantes, 356 pp.

Leyreloup, A.F., 1974. Les enclaves catazonales remontées par les éruptions néogènes de France: nature de la croûte inférieure. I. Lithologie et structurologie d'ensemble du complexe granulito-charnockitique sous-jacent au Massif Central français d'après les enclaves remontées par les volcans néogènes. Contrib. Mineral. Petrol. 46, 17–27.

Leyreloup, A.F., Dupuy, C., Andriambololona, R., 1977. Catazonal xenoliths in French Neogene volcanic rocks: constitution of the lower crust. Contrib. Mineral. Petrol. 62, 283–300.

Ludwig, K.R., 1999. User's Manual for Isoplot/Ex Version 2.02, A Geochronological Toolkit for Microsoft Excel, vol. 1. Berkeley Geochronology Center Spec. Pub., Berkeley, USA. 46 pp.

Maier, W.D., Barnes, S.-J., 1998. Concentrations of rare earth elements in silicate rocks of the Lower, Critical and Main Zones of the Bushveld Complex. Chem. Geol. 150, 85–103.

Mattauer, M., Matte, P., 1998. Le bassin Stéphanien de St-Etienne ne résulte pas d'une extension tardi-hercynnienne généralisée: c'est un bassin pull-apart en relation avec un décrochement dextre. Geodyn. Acta 11, 23–31.

Matte, P., 1986. Tectonics and plate tectonics model for the Variscan belt of Europe. Tectonophysics 126, 329–374.

Matte, P., 1991. Accretionary history and crustal evolution for the Variscan belt of Europe. Tectonophysics 196, 309–337.

Maury, R.C., Defant, M.J., Joron, J.-L., 1992. Metasomatism of the sub-arc mantle inferred from trace elements in Philippine xenoliths. Nature 360, 661–663.

McCulloch, M.T., Gamble, J.A., 1991. Geochemical and geodynamical constraints on subduction zone magmatism. Earth Planet. Sci. Lett. 102, 358–374.

McDonough, W.F., Sun, S.-S., 1995. The composition of the Earth. Chem. Geol. 120, 223–253.

Meissner, R., 1999. Terrane accumulation and collapse in central Europe: seismic and rheological constraints. Tectonophysics 305, 93–107.

Mercier, J.-C.C., 1972. Structure des péridotites en enclaves dans quelques basaltes d'Europe et d'Hawaii. Regards sur la constitution du manteau supérieur, Thèse 3ème cycle, Univ. Nantes, 229 pp.

Miyashiro, A., 1974. Volcanic rocks series in island arcs and active continental margins. Am. J. Sci. 274, 321–355.

Müntener, O., Kelemen, P.B., Grove, T.L., 2001. The role of H_2O during crystallization of primitive arc magmas under uppermost mantle conditions and genesis of igneous pyroxenites: an experimental study. Contrib. Mineral. Petrol. 141, 643–658.

Pearce, J.A., 1983. Role of the sub-continental lithosphere in magma genesis at active continental margins. In: Hawkesworth, C.J., Norry, M.J. (Eds.), Continental Basalts and Mantle Xenoliths, Shiva. Cheshire, UK, pp. 230–249.

Pharaoh, T.C., 1999. Paleozoic terranes and their lithospheric boundaries within the Trans-European Suture Zone (TESZ): a review. Tectonophysics 314, 17–41.

Pin, C., Joannon, S., 1997. Low level analyses of lanthanides in eleven silicate rock reference materials by ICP-MS after group separation using cation-exchange chromatography. Geostand. Newsl. 21, 43–50.

Pin, C., Paquette, J.-L., 2002. Sr–Nd isotope and trace element evidence for a Late Devonian active margin in northern Massif Central (France). Geodyn. Acta 15, 63–77.

Pin, C., Sills, J.D., 1986. Petrogenesis of layered gabbros and ultramafic rocks from Val Sesia, the Ivrea Zone, NW Italy:

trace element and isotope geochemistry. In: Dawson, J.B., Hall, J., Carswell, D.A., Wedepohl, K.H. (Eds.), The Nature of the Lower Continental Crust. Geol. Soc. London, Spec. Publ., vol. 24, pp. 231–249.

Porcelli, D.H., O'Nions, R.K., O'Reilly, S.Y., 1986. Helium and strontium isotopes in ultramafic xenoliths. Chem. Geol. 54, 237–249.

Prost, A.E., Becq-Giraudon, J.F., 1989. Evidence for mid-Permian compressive tectonics in Western Europe supported by a comparison with the Alleghanian geodynamic evolution. Tectonophysics 169, 333–340.

Prouteau, G., Scaillet, B., Pichavant, M., Maury, R.C., 1999. Fluid-present melting of ocean crust in subduction zones. Geology 27, 1111–1114.

Rubatto, D., 2002. Zircon trace element geochemistry: partitioning with garnet and the link between U–Pb ages and metamorphism. Chem. Geol. 184, 123–138.

Scambelluri, M., Philippot, P., 2001. Deep fluid in subduction zones. Lithos 55, 213–227.

Schmidberger, S.S., Hegner, E., 1999. Geochemistry and isotope systematics of calc-alkaline volcanic rocks from the Saar–Nahe basin (SW Germany)—implication for late-Variscan orogenic development. Contrib. Mineral. Petrol. 135, 373–385.

Streckeisen, A.L., 1974. Classification and nomenclature of plutonic rocks. Geol. Rundsch. 63, 773–786.

Totland, M., Jarvis, I., Jarvis, K., 1992. An assessment of dissolution techniques for the analysis of geological samples by plasma spectrometry. Chem. Geol. 95, 35–62.

Tribuzio, R., Thirlwall, M.F., Messiga, B., 1999. Petrology, mineral and isotope geochemistry of the Sondalo gabbroic complex (Central Alps, Northern Italy): implications for the origin of post-Variscan magmatism. Contrib. Mineral. Petrol. 136, 48–62.

Vander Auwera, J., Bologne, G., Roelandts, I., Duchesne, J.-C., 1998. Inductively coupled plasma-mass spectrometric (ICP-MS) analysis of silicate rocks and minerals. Geol. Belg. 1, 49–53.

Vidal, P., Dupuy, C., Maury, R., Richard, M., 1989. Mantle metasomatism above subduction zones: trace element and radiogenic isotope characteristics of peridotite xenoliths from Batan Island (Philippines). Geology 17, 1115–1118.

Voshage, H., Hoffmann, A., Mazzucchelli, M., Rivalenti, G., Sinigoi, S., Raczek, I., Demarchi, G., 1990. Isotopic evidence from the Ivrea Zone for a hybrid lower crust formed by magmatic underplating. Nature 347, 731–736.

Whitehouse, M.J., Platt, J.P., 2003. Dating high-grade metamorphism—constraints from rare-earth elements in zircon and garnet. Contrib. Mineral. Petrol. 145, 61–74.

Whitehouse, M.J., Claesson, S., Sunde, T., Vestin, J., 1997. Ion microprobe U–Pb zircon geochronology and correlation of Archean gneisses from Lewisian complex of Gruinard Bay, northwestern Scotland. Geochim. Cosmochim. Acta 61, 4429–4438.

Whitehouse, M.J., Kamber, B.S., Moorbath, S., 1999. Age significance of U–Th–Pb zircon data from early Archean rocks of west Greenland—a reassessment based on combined ion-microprobe and imaging studies. Chem. Geol. 160, 201–224.

Wiedenbeck, M., Alle, P., Corfu, F., Griffin, W.L., Meier, M., Oberli, F., Von Quadt, A., Roddick, J.C., Spiegel, W., 1995. Three natural zircon standards for U–Th–Pb, Lu–Hf, trace elements and REE analyses. Geostand. Newsl. 19, 1–23.

Zeyen, H., Novak, O., Landes, M., Prodehl, C., Driad, L., Hirn, A., 1997. Refraction-seismic investigations of the northern massif Central (France). Tectonophysics 275, 99–117.